The Thesis Committee for Dong Hee Song
Certifies that this is the approved version of the following thesis:

Using Simple Models to Describe Oil Production From Unconventional Reservoirs

APPROVED BY
SUPERVISING COMMITTEE:

Supervisor:

Larry W. Lake

Robert B. Gilbert

Using Simple Models to Describe Oil Production From Unconventional Reservoirs

by

Dong Hee Song, B.S.C.E

Thesis

Presented to the Faculty of the Graduate School of

The University of Texas at Austin

in Partial Fulfillment

of the Requirements

for the Degree of

Masters of Science in Engineering

The University of Texas at Austin

May 2014

Dedication

To my:

Brother Dong Kwan Song

My parents Chung Rak Song and Mae Hyang Kim Song

Bling Song

Neil Agrawal

Ben Frederick

Nabi Niazmidin

Ryan Kim

Acknowledgements

I would like to thank Dr. Larry W. Lake and Dr. Robert B. Gilbert for the guidance and support throughout my graduate studies; you have made my graduate experience at The University of Texas at Austin overwhelmingly positive. You have supported me with tremendous technical knowledge and unwavering patience.

I am also thankful to The Center for Petroleum Asset Risk Management for supporting my research financially. Also I would like to thank Shah Kabir of Hess for providing the dataset needed for my studies.

Finally, I would like to express gratitude to my family you have given me encouragement, unyielding support, and love.

Thank you.

Abstract

Using Simple Models to Describe Oil Production From Unconventional Reservoirs

Dong Hee Song, M.S.E.

The University of Texas at Austin, 2013

Supervisor: Larry W. Lake

Shale oil (tight oil) is oil trapped in low permeability shale or sandstone. Shale oil is a resource with great potential as it is heavily supplementing oil production in the United States (U.S. Energy Information Administration, 2013).

The shale rock must be stimulated using hydraulic fracturing before the production of shale oil. When the hydrocarbons are produced from fractured systems, the resulting flow is influenced by the fracture, the stimulated rock, and the matrix rock. The production decline rates from shale oil reservoirs experience flow regimes starting with fracture linear flow (fracture dominated), then bilinear flow (fracture and stimulated rock dominated), then formation linear flow (stimulated rock dominated), and finally pseudo-radial flow (unstimulated matrix rock dominated) (Cinco-Ley 1982).

In this thesis, daily production rates from a shale oil reservoir are modeled using a simple spreadsheet-based, finite difference serial flow simulator that models the single-phase flow of a slightly-compressible oil. This simulator is equivalent to flow through

multiple tanks (subsequent part of the thesis will call these *cells*) through which flow passes serially through one tank into the other. The simulator consists of 11 tanks. The user must specify the compressibility-pore volume product of each tank and the transmissibility that governs flow from one tank to another. The calculated rate was fitted to the given data using the Solver function in Excel. The fitted matches were excellent.

Although we can adjust all 22 parameters (2 per cell) to affect the simulation results, we found that adjusting only the first three cells nearest to the well was sufficient. In many cases, only two cells were enough. Adjusting 4 or more cells resulted in non-unique matches. Furthermore, the properties of the very first cells proved insensitive to the matches when using the 3 cells to match the data. The cells in the 2 cell model represent the stimulated zone and the unstimulated rock. Likewise, the cells in the 3 cell model represent the hydraulic fracture, the stimulated zone, and the unstimulated rock.

The accessed pore volume and transmissibility were responsive to the injected sand mass and fluid volume up to approximately 10^6 kg and 7000 m^3 respectively; injecting more sand and fluids than this caused negligible increases in the accessed pore volume and transmissibility. This observation suggests that the sand does not migrate far into the fractures. Similarly, it was observed that the number of stages was positively correlated with cell transmissibility and pore volume up to 20 stages. These results suggest that fracture treatments were significantly over designed and injecting less sand and water in fewer stages would optimize the economics of similar projects. To our knowledge this is the first work to analyze the results of fracture treatments by matching with pore volumes and transmissibility in a simple serial cell flow.

TABLE OF CONTENTS

List of Tables

List of Figures

CHAPTER 1: INTRODUCTION

1.1 Introduction

Shale oil (tight oil) is oil trapped in low porosity and permeability rock; oil that is already formed trapped in low permeability shale formations or tight sandstone. Shale oil is a resource with great potential as it is heavily supplementing oil production in the United States (U.S. Energy Information Administration, 2013).

When hydrocarbons are produced in fractured systems, the resulting flow is influenced by the fracture, the stimulated rock, and the matrix rock. The initial decline of a fractured reservoir is faster than the initial decline of a conventional reservoir, and the late time decline of a fractured reservoir is slower than that of a conventional reservoir. When flow from fractured shale systems is modeled using the Arps decline model, the result is often a b greater than 1 (Kanfar et al. 2012); this is a nonphysical value as b greater than 1 implies that the ultimate recovery is infinite. As such, modeling flow can be tricky.

Fractured systems have this unconventional flow behavior because of flow regimes. The flow regimens are fracture linear flow, bilinear flow, formation linear flow, and pseudo-radial flow.

- Fracture linear flow is the flow regime where the flow is dominated by the flow inside of the fracture. As the pressure has not “seen” anything beyond the fracture, this is a linear flow (Cinco-Ley, 1982).
- Bilinear flow is the superposition of fracture flow and linear flow into the fracture from the surrounding (Cinco-Ley, 1982).

- Formation linear flow is the flow is dominated by the linear flow of fluid into the fracture(Cinco-Ley, 1982).
- Pseudo-radial flow occurs when the drainage from the formation linear flow expands into a nearly radial shape(Cinco-Ley, 1982).

Various methods have been used in an effort to model fractured flow; the methods can be broadly divided into three groups: analytic models, complex simulations, and simple models. Some analytic models that were used to model fractures are the Arps decline curve analysis (1945) and Valko's stretched exponential method. While these analytic models do a good job matching the flow regimes, no estimations for reserves or fracture parameters can be gained by working with the analytic models. Complex simulations can also yield good modeling of the data. But complex simulation has key weaknesses such as insufficient geological data, insufficient knowledge about the fracture system, and the computing power demand is large. Simple models can succeed where the analytical models and complex simulations fail by providing estimations for physical parameters, managing uncertainty, and having fast run times.

The simple model selected for this study is a Microsoft Excel® based 1-D flow simulator with 11 serial cells. Using this simulator and conceptual models, three models that describe the production from fractured systems were developed: 4-Cell Model, 2-Cell Model, and 3-Cell Model. These models were used to model real production data from a fractured shale play.

Relationships between the model fitting parameters (pore volume and transmissibility of cells) and well summary information (initial productivity index, age of well, number of stages, total fluid injected, and total sand injected) were found.

1.2 Research Objectives

The research objectives are as follows:

1. Study the provided data set.
2. Pick out key flow characteristics to model with a simple model.
3. Develop simple models which will model flow from fractured systems (series model).

1.3 Outline of Thesis

Chapter 1 will introduce the research interest, problems, and the solution approach used in this study. Chapter 2 introduces the problem in greater detail providing background information and the basis of the solution used in this study.

Chapter 3 describes the production data from a fractured shale oil play that was used in this study.

Chapter 4 discusses the simulator used to model unconventional fractured flow.

Chapter 5 discusses the pre-modeling sensitivity study done to the simulator to better understand the simulator.

Chapter 6discusses the models that were used for this study.

Chapter 7 presents the results of this study.

Chapter 8 summarizes the study, lists conclusions, and suggests future work to be done to further the study.

CHAPTER 2: BACKGROUND

2.1 Shale oil

Shale oil is not to be confused with oil shale. Shale oil (tight oil) is oil trapped in low porosity and permeability rock. Oil shales are rocks with large kerogen content; essentially rocks with oil producing potential that never became hot enough to convert its kerogen to oil. The most characteristic technique to produce oil shale is to heat it up in an oxygenless environment. Shale oil is oil that is already formed trapped in low permeability shale formations or tight sandstone.

Normal drilling and completion techniques are uneconomical in shale oil projects because of low permeability and other shale rock characteristics; this makes shale oil an unconventional resource.

Horizontal drilling and hydraulic fracturing (frac-jobs) are used together to access the tightly locked hydrocarbons and make shale oil projects economical. In this section, the availability of U.S. shale oil and shale rock properties are discussed.

Table 1: Drilling Permits issued in the Eagle Ford(Texas Railroad Comission, 2013)

Year	Drilling Permits Issued
2008	26
2009	94
2010	1,010
2011	2,826
2012	5,230

Table 2: U.S. Crude Oil Production (Average, thousands of barrels per day)(U.S. Energy Information Adminstration, 2013)

State	2007	2008	2009	2010	2011	2012
Texas	1,072	1,109	1,094	1,168	1,453	1,997
Gulf of Mexico	1,282	1,156	1,562	1,544	1,316	1,265
North Dakota	124	172	218	310	419	662
California	599	586	567	552	531	532
Alaska	722	683	645	601	561	526
Oklahoma	175	184	183	186	213	243
New Mexico	162	164	168	179	196	230
Louisiana	211	198	189	185	189	193
Wyoming	148	145	141	146	150	158
Colorado	71	80	83	89	107	130
Kansas	100	108	108	111	114	119
Utah	54	60	63	68	72	82
Montana	96	86	76	69	66	71
Mississippi	57	63	65	66	66	66
Others	204	206	192	195	198	206
Total	5,077	5,000	2698	5469	4198	3218

Shale oil production in the United States shows great potential; over 4000 new producing wells began production in the U.S.(Zhou et al. 2013). This potential for shale oil can be seen again in the increasing number of drilling permits issued in the Eagle Ford formation from 2008~2012 as seen in Table 1. It is also observed in

Table 2 that the oil production in North Dakota, Texas, and Colorado has increased significantly from 2007 to 2012 while other states did not see much growth. Table 3 states that most of the growth in Texas, N. Dakota, and Colorado came from the production of shale oil. Such trends of growth in shale oil demonstrate the hydrocarbon potential.

Table 3: Shale Oil Production Contributions From: Eagle Ford, Bakken, and Niobrara(North Dakota Department of Mineral Resources, 2013; Texas Railroad Comission, 2013; Eisinger et al. 2012)

Formation	2008	2009	2010	2011	2012
Texas Eagle Ford	0.352	0.843	15	129	400
North Dakota Bakken	75	136	235	352	599
Colorado Niobrara	0.228	0.503	3	15	11

Formations bearing shale oil include the Bakken Shale, Barnett Shale, Niobrara Formation, and the Eagle Ford Shale. Such formations have been discovered as early as 1970 in the Niobrara Formation and 1986 in the Bakken Formation (Sonnenberg, 2013; Tran et al. 2011). However, only recently have these plays emerged as economic prospects because of developments in technology. A map of the major U.S. shale basins is shown in Figure 1.

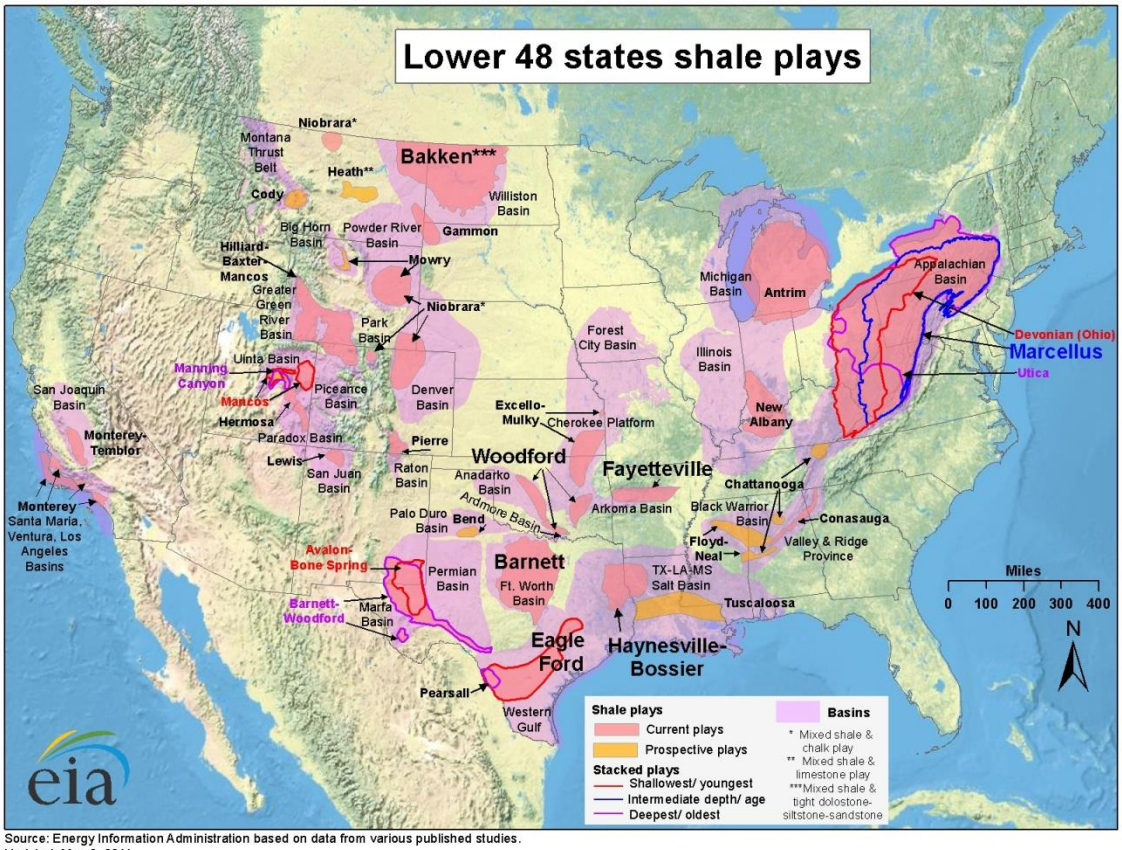

Source: Energy Information Administration based on data from various published studies.
Updated: May 9, 2011

Figure 1: Shale Plays In Lower 48 States(Energy Information Administration, 2011)

Shale oil can migrate into a shale formation or be formed inside of the shale rock. The Middle Bakken formation did not generate its own oil but has had oil migrate from the Upper Bakken and the Lower Bakken formations (Kumar et al. 2013). The Eagle Ford Formation is an example of shale being its own source rock; a self-sourcing reservoir (Tian et al. 2013).

Table 4 summarizes the rock properties of the Bakken Shale, Barnett Shale, Niobrara Formation, and the Eagle Ford Shale plays.

Table 4: Properties of Bakken, Barnett, Niobrara and Eagle Ford Formations(Tran et al. 2011; Besler et al. 2007; Tian et al. 2010; Zhou et al. 2013; Sonnenberg, 2013; Tian et al. 2013; Zhou et al. 2013)

Formation	**Bakken Shale**	**Barnett Shale**	**Niobrara**	**Eagle Ford**
Lithology	Sand stone, limestone, siltstone	Shale, siliceous mudstone, marly carbonate, limestone	Calcareous shale, shaly limestone, marls, limestone	Overlies: Buda Limestone, Underlies: Austin Chalk Shale, Dolomite
Matrix Permeability (md)	0.0003-3.36	1.87E-07-0.0003	0.001-5.0	3.17E-06-0.061*
Porosity φ (fraction)	0.075	-	0.06-0.5	-
Formation compressibility, $c_f(psi^{-1})$	3.00E-06	-	-	-

*note: Eagle Ford samples contained cracks

2.2 Technologies to Produce Shale Oil

Horizontal drilling and hydraulic fracturing are the two most important technologies that cause shale oil production to be economic. Together, horizontal drilling and fracturing aims to (as seen in Figure 2):

- Access much of the reservoir while isolating zones that should be isolated (isolate reservoir from groundwater).
- Stimulate shale rock to increase reservoir access even further.

In this section the reasons why horizontal drilling and hydraulic fractures make shale oil production economical and the attributes of the horizontal paths and the fractures are discussed.

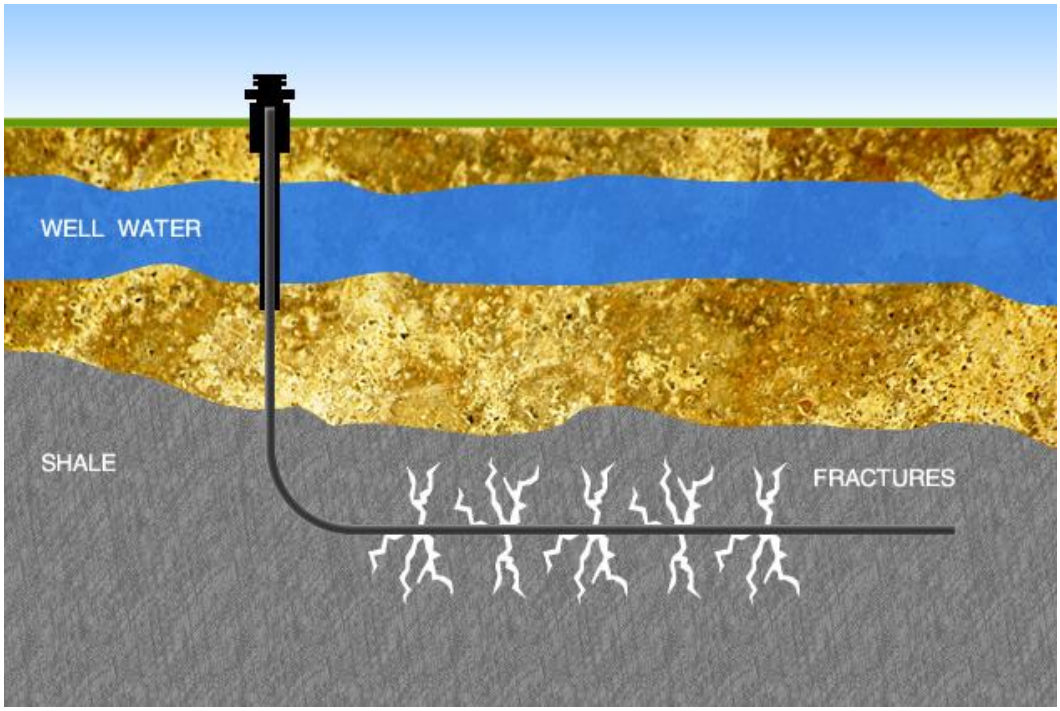

Figure 2: Idealized Cross Section of Horizontal Drilling and Creation of Fractures for Increased Oil and Gas Recovery (Foran, 2011)

Horizontal drilling is process that involves maneuvering of the drill path to result in greater contact with the producing zone. As horizontal drilling results in a well having extended contact with the reservoir, many sections (stages), of the well can be perforated and stimulated. These stages can be analogous to having many vertical wells along the well path. In the Bakken and Eagle Ford formations, the length of the laterals can be around 2000 to 6000 ft(Tran et al. 2011; Spencer et al. 2013). In the Bakken formation, Tran et al. (2011) points out that from 1953 to 1987, 11.5 million STB of oil and 12.5 Bcf of gas were produced using vertical wells; while from 1987 to 2010, 131.3 million STB of oil and 131.017 Bcf of gas were produced according to the Drillinginfo database. It is known that horizontal drilling was used in the Bakken formation during more recent times indicating the effectiveness of horizontal drilling. Similarly, Tianet al. (2010) mentions that in the Barnett Shale formation, horizontal wells produce approximately twice as much oil and gas compared to the production of vertical wells in 5 Barnett production regions.

Hydraulic fracturing is a technology that artificially creates fractures in rock and props it open with proppants to achieve a greater drainage area for more favorable hydrocarbon production. A successful frac-job will stimulate a large volume of rock and create large fractures that are held open by proppants. Proppants are particles used to "prop" open the fracture even after the fluid pressure from the hydraulic fracturing has dissipated; in this study, sand was the proppant of choice. This successful frac-job will then result in fractures and stimulated volumes that have much greater permeability than the surrounding rock (matrix). The permeability difference is one of the reasons why

flows in fractured systems are different from conventional flow; the flow is further discussed in the next section and throughout this thesis.

Although there have been many efforts to understand the nature of the fractures and the stimulated volume, the exact properties are incompletely understood. Attempts made to investigate the properties of these fractures include:(Paige et al. 1992) Using hydraulic impedance testing to measure fracture dimensions; (Mills et al. 2004) Measuring the stress change around a full size hydraulic fracture to measure fracture growth. Fracture simulators can use values reported in Table 5 for post frac-job systems in shale.

Table 5: Typical Post Hydraulic Fracture Parameters(Zhang, et al. 2009)

Conductivity (md-ft)	1 - 50
Fracture Spacing (ft)	200 - 600
Fracture width (ft)	0.01
Fracture Height (ft)	up to 300
Fracture Half-Length (ft)	100 - 500
Fractures Per Well	5 - 15

The values in Table 5 are consistent with the values that were estimated using the 1-D simulator in this thesis.

2.3 Flow Regimes

When hydrocarbons are produced in fractured systems, the resulting flow is influenced by the fracture, the stimulated rock, and the matrix rock. This flow does not match the flow characteristics of a conventional reservoir which typically have larger permeability and porosity compared to a tight system. When flow from fractured shale systems is modeled using the Arps decline model, the result is often a b greater than 1 (Kanfar et al. 2012); this is a nonphysical value as b greater than 1 implies that the ultimate recovery is infinite. This unconventional flow characteristic is likely because the different flow regimes that exist in flow in fractured systems. In this section factors that affect flow regimes and evidence of flow regimes are discussed.

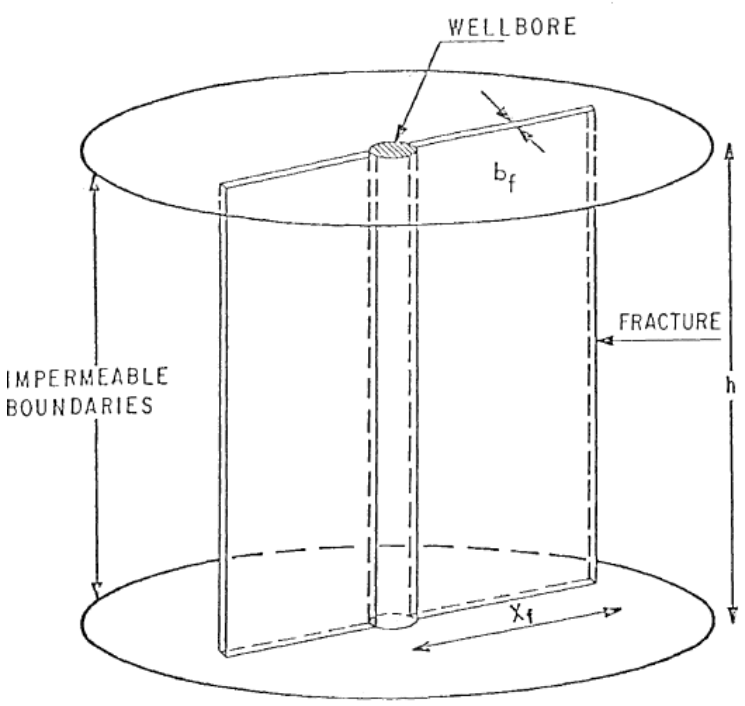

Figure 3: Finite Conductivity Vertical Fracture in Infinite Slab Reservoir (Cinco-Ley, 1982)

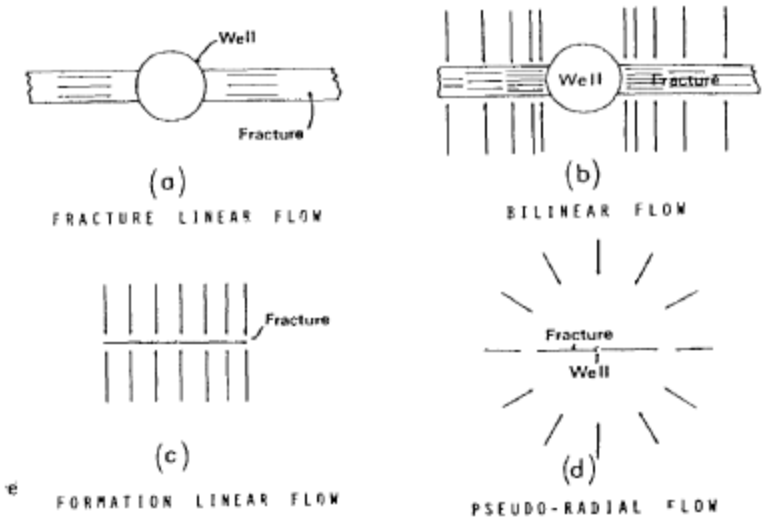

Figure 4: Flow Periods for a Vertical Fracture (Cinco-Ley, 1982)

Single bi-wing fracture systems can be visualized as in Figure 3. Such a system would have a wellbore, a bi-wing fracture growing from the wellbore, and matrix rock around the entire system. The fracture would have dimensions of: a fracture width-b_f, a fracture length-x_f, a fracture permeability-k_f, and a system height-h. Ideally, the fracture in this system should have a much greater permeability than the matrix rock. When such conditions are met, the flow will exhibit four distinct flow regimes: fracture linear flow, bilinear flow, formation linear flow, and pseudo-radial flow (Cinco-Ley, 1982).

- Fracture linear flow is the flow regime where the flow is dominated by the flow inside of the fracture (see Figure 4-a). As the pressure has not "seen" anything beyond the fracture, this is a linear flow. Fracture linear flow can be determined as the straight line portion on a *Change in pressure vs. square root of time* (Δp vs $\sqrt{t}$) plot using a semi log axis; this would mean a ½ unit slope on a *Change in pressure vs time* plot (Δp vs t) using a log-

log axis (Cinco-Ley, 1982). The derivation supporting a linear Δp vs $\sqrt{t}$ relationship is in Appendix F.

- Bilinear flow is the superposition of fracture flow and linear flow into the fracture from the surrounding rock (see Figure 4-b). Fracture linear flow can be determined as the straight line portion on a *Change in pressure vs. fourth root of time* (Δp vs $\sqrt[4]{t}$) plot using a semi log axis; this would mean a ¼ unit slope on a *Change in pressure vs time* plot (Δp vs *t*) using a log-log axis (Cinco-Ley, 1982).
- Formation linear flow is the flow that is dominated by the linear flow of fluid into the fracture (see Figure 4-c). Formation linear flow can be determined as the straight line portion on a *Change in pressure vs. square root of time* (Δp vs $\sqrt{t}$) plot using a semi log axis; this would mean a ½ unit slope on a *Change in pressure vs time* plot (Δp vs *t*) using a log-log axis (Cinco-Ley, 1982).
- Pseudo-radial flow occurs when the drainage from the formation linear flow expands into a nearly radial shape (see Figure 4-d). Pseudo-radial flow can be determined as the straight line portion of Δp vs log(*t*) plot; this would mean an unit slope on a *Change in pressure vs time* plot (Δp vs *t*) using a log-log axis (Cinco-Ley, 1982).

Not all of the flow regimes are visible in the flow data; in the case of low permeability fractures ($k_f b_f \leq 0.1$), only the bilinear flow and pseudo-radial flow are

exhibited (Cinco-Ley et al. 1987). Also, the data may not extend long enough to express all of the flow regimes.

As discussed earlier, these flow regimes are most evident when plotted in a log-log Δp vs *t* plot. In a study to analyze production data from tight oil wells, (Kabir et al. 2011) plots Productivity index(J) vs *t*; where J is defined as:

$J = \Delta P/q,$ where q is production rate and ΔP is the pressure drop

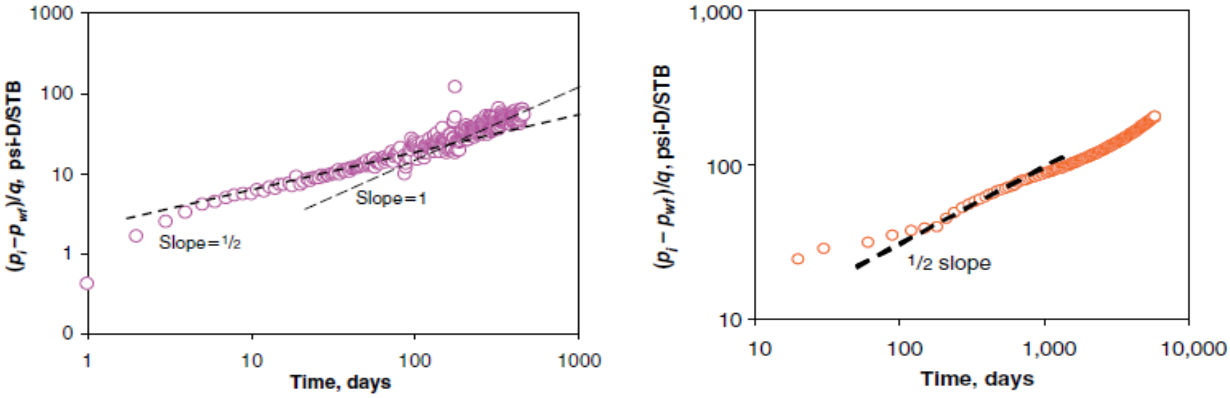

Figure 5: Data Demonstrating Flow Regimes (left: Production data, right: artificial data)(Kabir, et al. 2011)

In Figure 5 the evidence of the flow regimes are seen in the straight line portions with the ½ unit slope and the unit slope respectively. Various methods are used to model such behavior.

2.4 Techniques Used to Model Oil Production

Flows from fractured shale systems are unconventional; in unconventional tight oil, the production decline rate is much larger at early times and much lower at late times compared to that of conventional oil. Various methods have been used in an effort to address this challenge; the methods can be broadly divided into three groups: analytic models, complex simulations, and simple models. This section will discuss the three model types mentioned.

2.4.1 Decline curve analysis and Valko's stretched exponential model

Common analytical models used to model fractured flow include the traditional decline curve analysis(Arps, 1945) and Valko's stretched-exponential method (Valko, 2009). The equation expression of the Arps model for flow rate is provided in Equation 1 (Arps, 1945).

$$\boldsymbol{q(t)} = \frac{\boldsymbol{q_i}}{\boldsymbol{(1+bD_i t)^{\frac{1}{b}}}} \qquad (1)$$

q is flow rate, q_i is initial flow rate, D_i is the initial decline rate, and b is the hyperbolic factor ($0 \leq b \leq 1$). When b=0, the decline curve take the form of exponential decline, and when b=1, the decline curve take the form of harmonic decline. When b is not between 0 and 1, it is considered nonphysical as b greater than 1 implies infinite ultimate recovery.

Decline curve analysis is used extensively in conventional fields; however, when flow from fractured shale systems is modeled using the Arps decline model, the result is often a b value greater than 1 (Kanfar et al. 2012). To address such issues, modified models such as Valko's stretched-exponential method were developed. Valko's stretched-

exponential method for modeling flow rate takes the equation form of Equation 2 (Valko, 2009).

$$\boldsymbol{q = q_0 \exp[-\left(\frac{t}{\tau}\right)^n]} \quad (2)$$

$$\boldsymbol{\tau = \left(\frac{n}{D_1}\right)^{\frac{1}{n}}} \quad (3)$$

q is flow rate q_i is initial flow rate, n is a model parameter, and τ is a model parameter.

Analytical models are appealing as they are usually easy to use and fitting parameters can be used to fit the model to the data. The down side of the analytical model is that that they do not give estimates of reserves or give insight to reservoir characteristics.

2.4.2 Other analytic models

The use of analytical models to solve model shale oil production is further discussed in (Valko, 2009; Yuan et al. 2013;Kabir et al. 2011;Kanfar et al. 2012;Yu et al. 2013;Clark et al. 2011). Furthermore, analytical model studies done on shale gas production such as (Miller et al. 2010) offer insight into shale oil production. Other analytical models that are used to model fractured flow include but are not limited to: the power-law exponential method, transient productivity index, Duong's method, and logistic growth models (Kabir et al. 2011).

2.4.3 Numerical simulations

Complex numerical simulations are also used to model tight oil production data. The gridding is especially important when modeling the fractures (Timur, 2008). A fine grid is needed around the fractured zone to accurately model the flow, but the larger grid resolution means more computational time. Similarly, the time step should be small enough to model the flow, but not so small that it takes excessive simulation time.

A downside of simulations is that modern geological data and computational power are insufficient to develop a truly accurate model of the fractures (Timur, 2008). The use of reservoir simulation to model flow from fractured systems is discussed in (Agboada et al. 2013;Timur, 2008).

Simple numerical models discussed in this thesis attempt to address the shortcomings of both the analytical models and reservoir simulations. Zones that are thought to have similar flow characteristics were grouped to handle the uncertainty in geological data. In this thesis, the groups were modeled as tanks connected in serial form. More descriptions of the simple model are in Chapter 4.

CHAPTER 3: DATA

3.1 Overview

The data used in this study were comprised of a well data summary file, monthly production data file, and daily production data file. The daily data was obtained after the well data summary and the monthly production data; as such it was analyzed later. The data included:

- Well data summary (information from 804 wells)
  - ○Well name (disguised)
  - ○ Lateral type
  - ○ Orientation
  - ○ Formation (disguised)
  - ○ Initial water saturation [fraction]
  - ○ Total fluid volume injected [bbl]
  - ○ Porosity of formation1 [fraction]
  - ○ Overpressure of formation1 [psi]
  - ○ Initial number of stages
  - ○ Lateral length [ft]
  - ○ Spacing [ft]
  - ○ Water cut [fraction]
  - ○ Avg injection pressure [psi]
  - ○ Mass of sand injected [lbs]
  - ○ Pressure of formation 1 [psi]
  - ○ Depth to formation 1 [ft]
  - ○True vertical thickness both formations [ft]
  - ○ Average oil production rate after 30 days [stb/day]
  - ○ Average oil production rate after 60 days [stb/day]
  - ○ Average oil production rate after 90 days [stbday]
  - ○ Cumulative oil production after 30 days [stb]
  - ○ Cumulative oil production after 60 days [stb]
  - ○ Cumulative oil production after 90 days [stb]
  - ○ Cumulative water production after 30 days [stb]
  - ○ Cumulative water production after 60 days [stb]
  - ○ Cumulative water production after 90 days [stb]
  - ○ Cumulative total fluid production after 30 days [stb]
  - ○ Cumulative total fluid production after 60 days [stb]

    - Cumulative total fluid production after 90 days [stb]
    - Cumulative oil production after 30 days/stages [stb]
    - Cumulative oil production after 60 days/stages [stb]
    - Cumulative oil production after 90 days/stages [stb]
    - Cumulative water production after 30 days/stages [stb]
    - Cumulative water production after 60 days/stages [stb]
    - Cumulative water production after 90 days/stages [stb]
    - Cumulative total fluid production after 30 days/stages [stb]
    - Cumulative total fluid production after 60 days/stages [stb]
    - Cumulative total fluid production after 90 days/stages [stb]
- Monthly production data (information from 862 production wells)
    - Well name (disguised)
    - Time [month]
    - Oil production [stb]
    - Water production [stb]
    - Gas production [Mscf]
    - Days on production [days]
- Daily production data (information from 266 production wells)
    - Well name (disguised)
    - Time [days]
    - Oil production [stb]
    - Water production [stb]
    - Gas production [cf]
    - Tubing pressure [psi]
    - Initial number of stages
    - Formation name (disguised)

The data was made anonymous by replacing the well names with UT ID's. Also, the formation names were changed.

As porosity, pressure, overpressure, and depth of only formation 1 was given, only wells that were producing from this formation were analyzed.

3.2 Monthly Data

For the initial analysis, the data were filtered to pick out wells that demonstrated good decline curve patterns. The wells that had fewer than 40 data points, wells that showed large jumps and wells that did not correspond to wells in the summary data were removed for this initial study. Figure 6is an example of a well with a large jump; the jump is likely to be caused by a work-over performed on the well. After the filtering, only 45 wells (out of the original 862 wells) remained for analysis; many wells had been filtered out because there less than 40 data points.

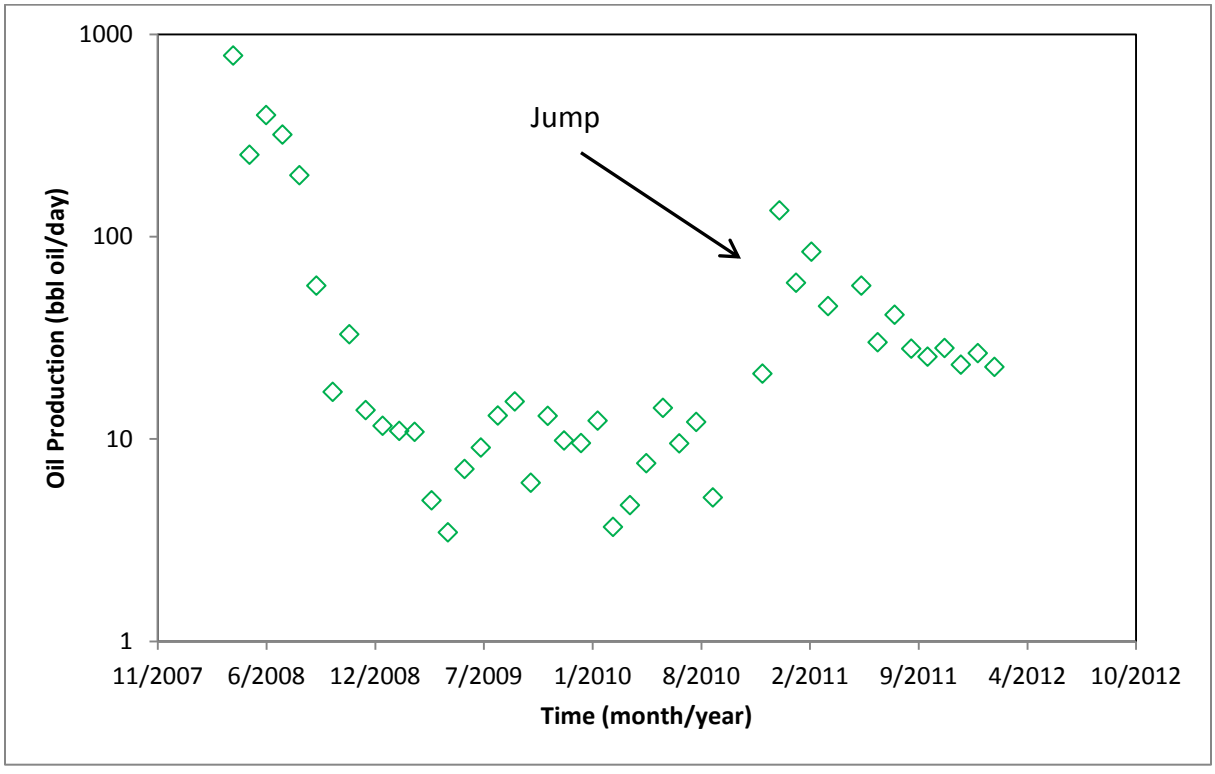

Figure 6: Example of Well With Large Jumps in Oil Production From Well UTID: 77

The wells in the monthly production data was matched with wells in the well summary data and stored in a relational database where the two were connected with the Well ID (primary key).

Although the decline of the production was not modeled using the monthly production data, information about the gas-oil-ratio and the water-oil-ratio were obtained from this data set.

Over 90% of the gas-oil-ratio (GOR) are less than 2 Mcf-gas/bbl-oil as seen in Figure 7. The GOR changed very little over time in all of the wells. This constant and low GOR justifies that the oil is the flowing phase between oil and gas. Also, this constant GOR implies that the average pressure of the reservoir did not drop below the bubble point as discussed in (Tran et al. 2011). If the average reservoir pressure did drop below the bubble point, a jump in GOR would have been observed.

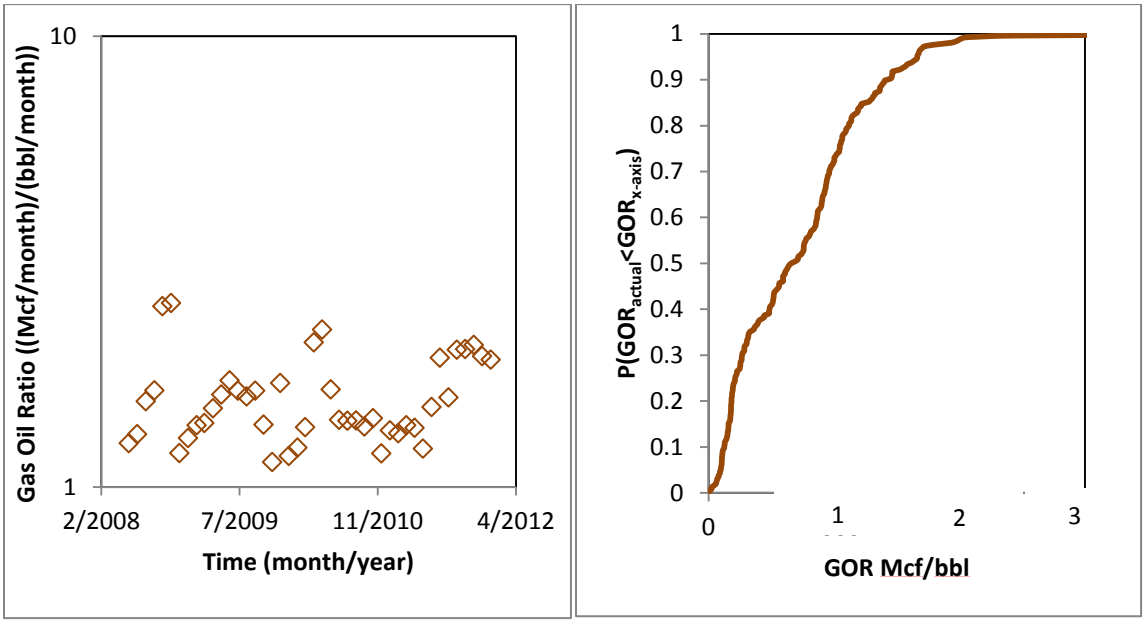

Figure 7: Typical Producing Gas Oil Ratio from Monthly Production Data From Well UTID: 44 (Left); CDF of Cumulative Gas-Oil Ratios (Right)

Over 85% of the water-oil-ratio (WOR) are less than 1 stb/stb as seen in Figure 8. Like the GOR, the WOR did not change much over time. If the water was flowing from an aquifer, an increasing WOR is expected as the oil rate would decline while the water rate remains consistent. This low and constant WOR supports the assumption that the oil phase is the flowing phase.

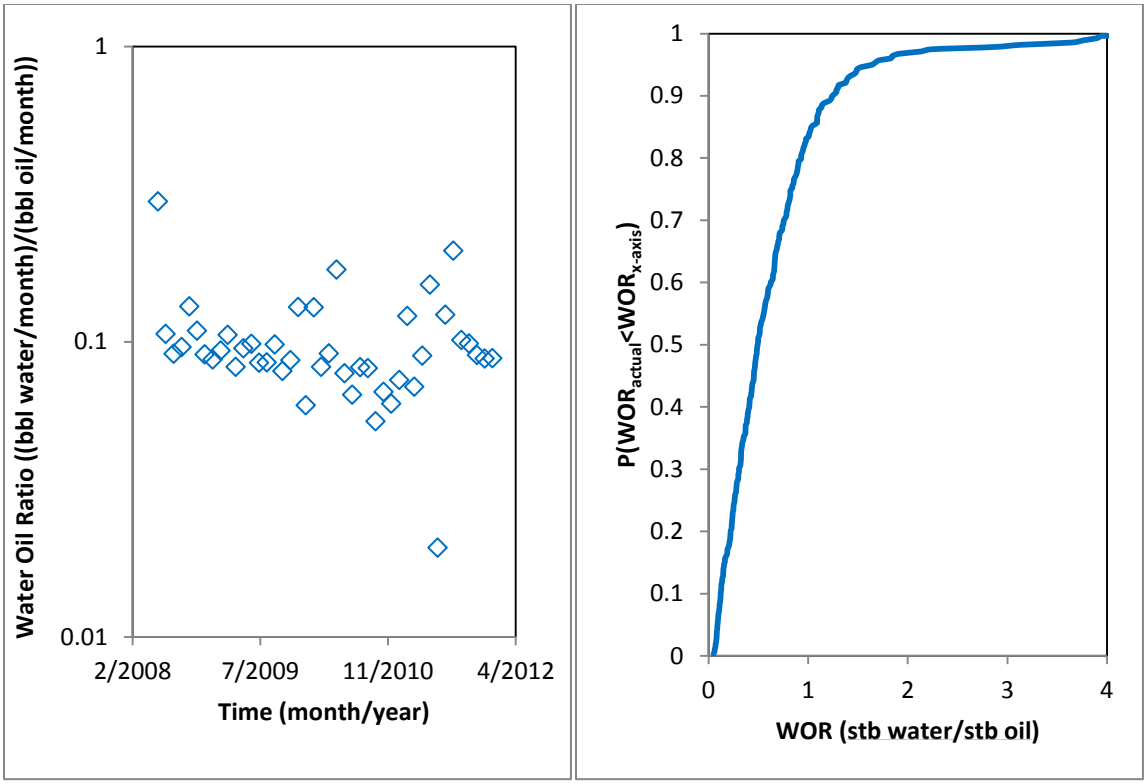

Figure 8: Typical Producing Oil Water Ratio from Monthly Production Data From Well UTID: 44 (Left); CDF of Cumulative Water-Oil Ratios (Right)

3.3 Daily Data

The daily production dataset was obtained to increase the number of data points to analyze. The daily production data originally contained production informationfrom266 wells; after the wells with less than 40 data points, wells with large jumps in the data, and wells with no well summary information were filtered out, 146 wells exhibiting analyzable decline trends remained. In the filtering of the daily production data, if the first part of the production was showing a smooth decline along with inconsistencies in the later part of the production, only the first part was kept for analysis. Even with the filtering, the some degree of scatter was expected in the filtered data; especially at the start of the production.

An example of a well exhibiting an analyzable decline curve is in Figure 9. All of the other graphs in Section 3.3 use the data from the well UTID: 4.

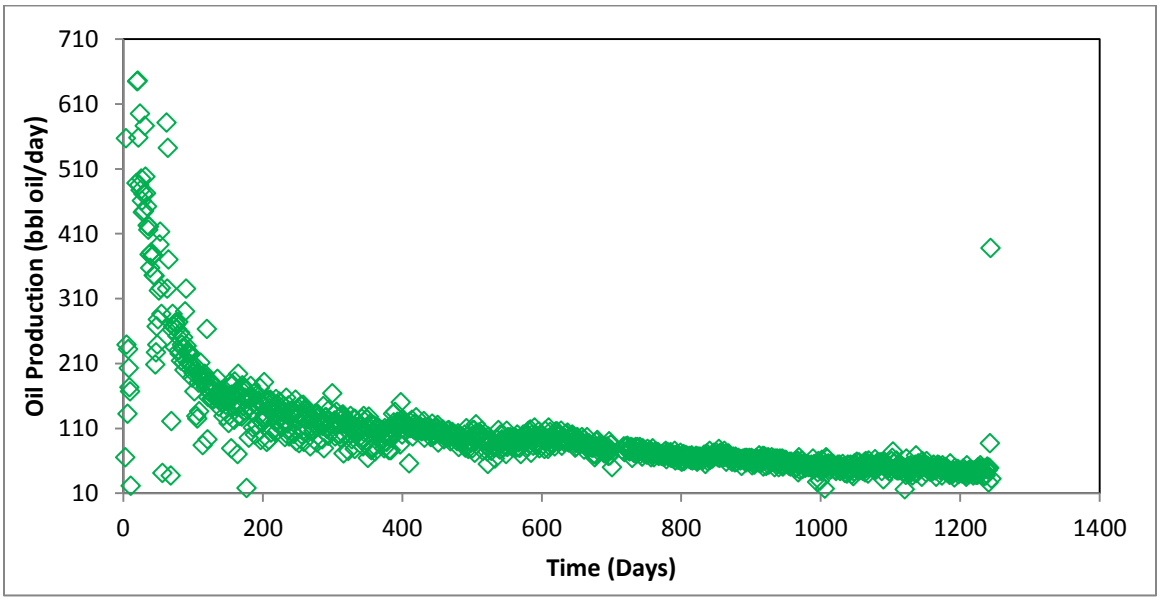

Figure 9: Example of Analyzable Oil Production Data From Well UTID: 4

The filtered data was plotted in various ways to look for trends in the data. The plots that made the various trends more visible are the oil production rate (log scale) vs. time (linear scale) plot, the oil production rate (log scale) vs. cumulative oil production (linear scale) plot, the total fluid production rate (log scale) vs. cumulative total fluid production (linear scale) plot, and 1/production rate (log scale) vs. time (log scale) plot.

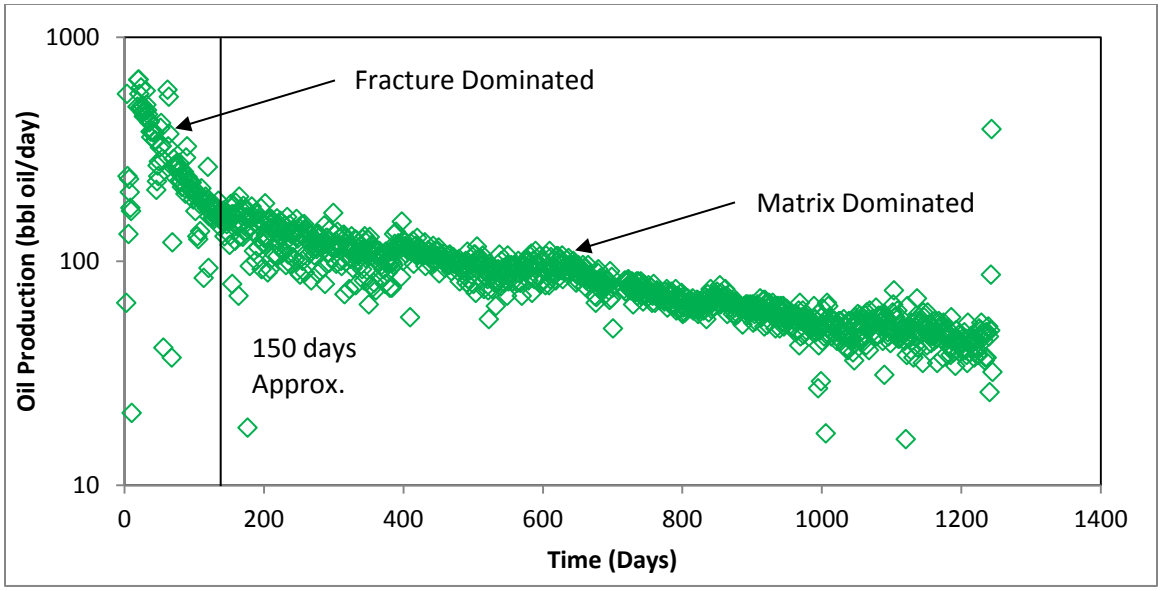

Figure 10: Oil Production (Log Scale) vs. Time (Linear Scale) From Well UTID: 4

In the oil production vs. time plot (Figure 10), two linear segments can be observed; a steep decline up to approximately 150 days, and a less steep decline after 150 days. Tran et al. (2011) have studied similar graphs on the Bakken Formation and concluded that the fast (early) decline is fracture dominated and the slower (later) decline is matrix dominated. The stimulated volume is likely to have a much greater permeabilty than the matrix so it makes sense that 2 flow regiemes are seen.

Straight line decline in the oil production rate (log scale) vs. time (linear scale) plot is associated with exponential decline.

The 150th day which is approximately the time when the flow regime changes is the day when the 34974th barrel of oil was produced from this well (cumulative production). This becomes important when looking at

Figure 11.

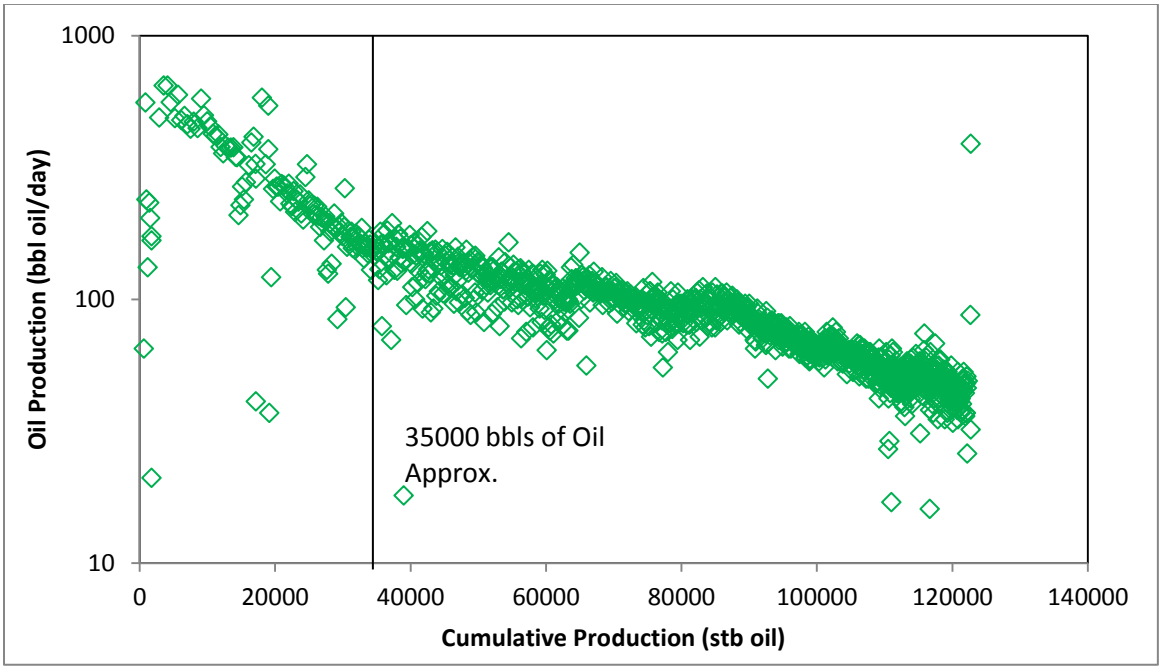

Figure 11: Oil Production (Log Scale) vs. Cumulative Oil Produced (Linear Scale) From Well UTID: 4

In the

Figure 11, two linear segments can again be observed. The flow regime changes at approximately 35000bbls of cumulative oil produced; fast decline rate before 35000bbls and slower decline rate after 35000bbls. The cumulative oil produced associated with the change in flow regime is when the date where the flow regime changes in Figure 10.

A straight line decline in the oil production rate (log scale) vs. cumulative production (linear) plot is associated with harmonic decline.

The total fluid (water and oil) production (log scale) vs. total fluid cumulative production (linear scale) plot (Figure 12).

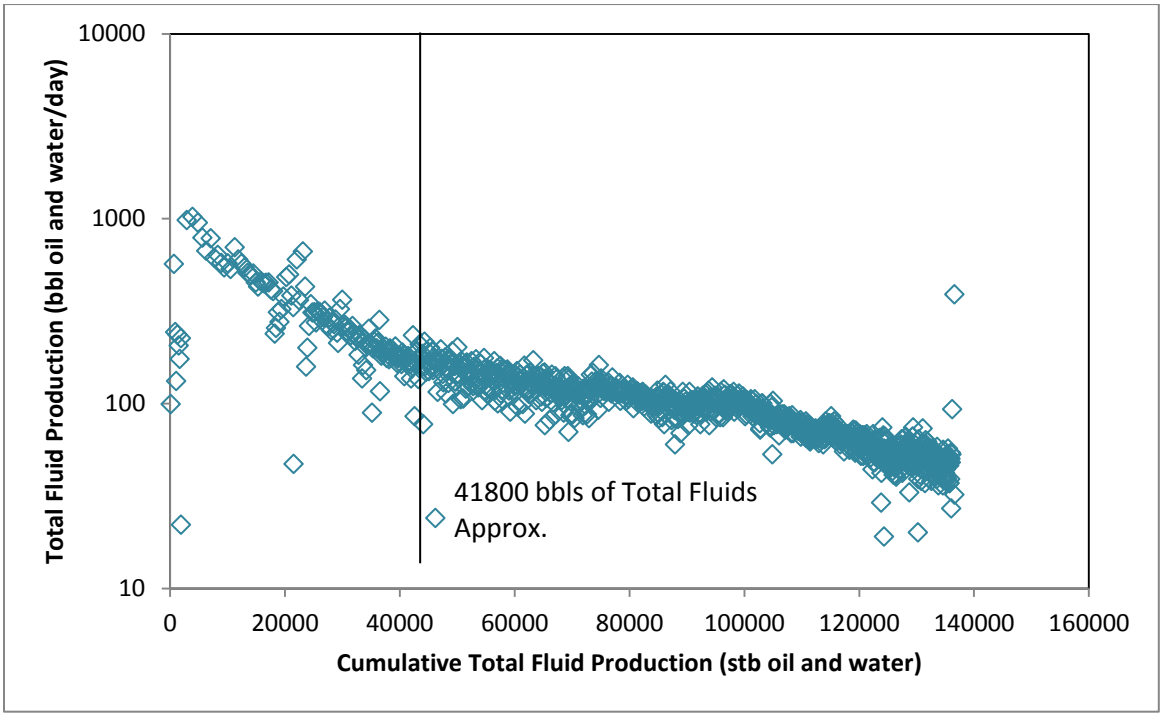

Figure 12: Total Fluid Production (Log Scale) vs. Cumulative Total Fluid (Water and Oil) Production (Linear Scale) From Well UTID: 4

The 150th day of production corresponds to 41800bbls of cumulative total fluid production. The trend of fast decline before 41800bbls of cumulative total fluid

production and slow decline after 41800bbls of cumulative total fluid prediction is consistent with observations made from Figures 10 and 11. This was expected as the water-oil ratio is constant.

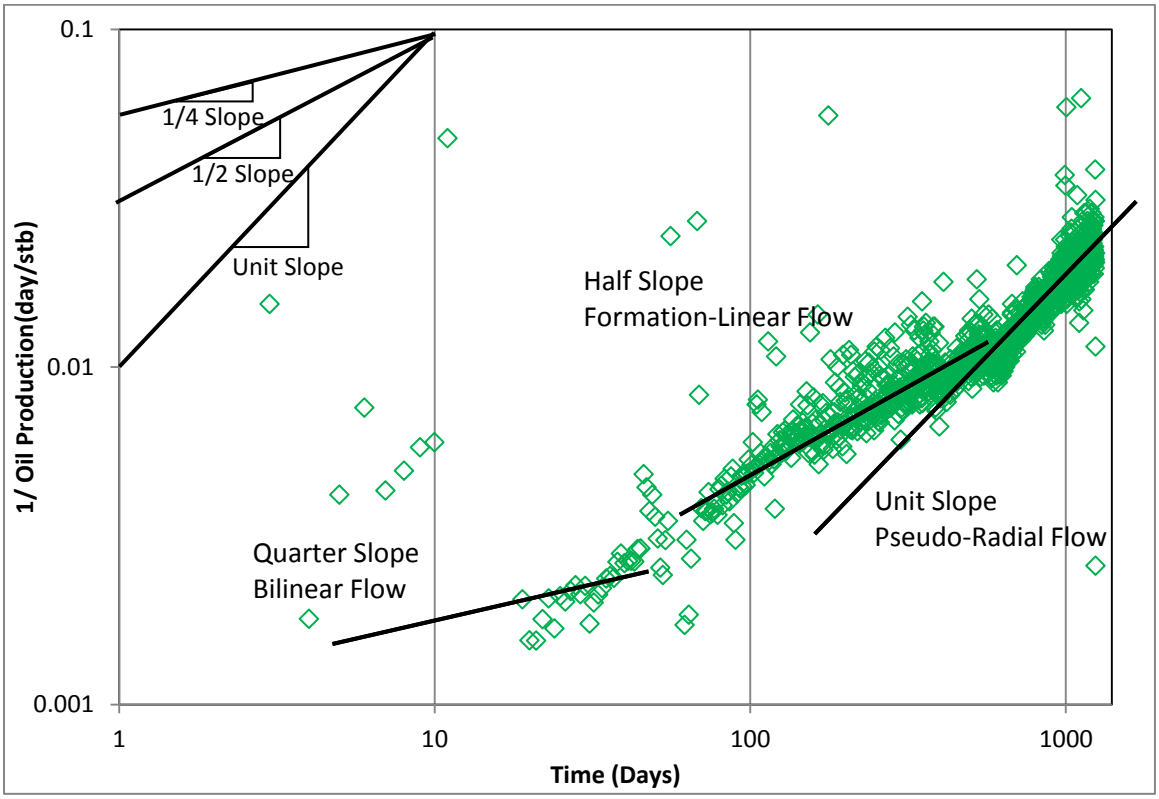

Figure 13: Reciprocal Oil Production (Log Scale) vs. Time (Log Scale) From Well UTID: 4

The reciprocal oil production vs. time plot was plotted in the place of the reciprocal productivity index vs. time (1/J vs. time) plot, which is the method to identify the flow regime as discussed in Cinco-Ley et al. (1982).Cinco-Ley et al. (1982) discusses the flow regimes that should be seen in fractured flow; at early time, fracture linear flow marked by a half slope on the 1/J vs. time plot is dominant, bilinear flow marked by a quarter slope on the 1/J vs. time plot follows the fracture linear flow, formation linear

flow marked by a half slope on the 1/J vs. time plot follows the bilinear flow, and pseudo-radial flow marked by a full slope on the 1/J vs. time plot follows the formation linear flow. The alteration from reciprocal productivity index vs. time to reciprocal oil production vs. time was made as bottom hole pressure data and average pressure data were unavailable.

Although the reciprocal oil production vs. time plot is not the method prescribed by Cinco-Ley et al. (1982), the linear segments with the quarter half and full slopes can be seen in the data. The quarter slope is associated with bilinear flow, the half slope with formation linear flow, and the full slope with pseudo-radial flow as discussed in Chapter 2 (visualized in Figure 4). The fracture linear flow associated with a half slope is missing in Figure 13.

Possible explanations for why the fracture linear flow is not observed include that the fracture linear flow happens very fast at the beginning of production, and/or during this time, production was choked. This evidence is seen in Figure 14; because the flow was being choked, the tubing head pressure during the first 40 days is much greater than the rest of the production history.

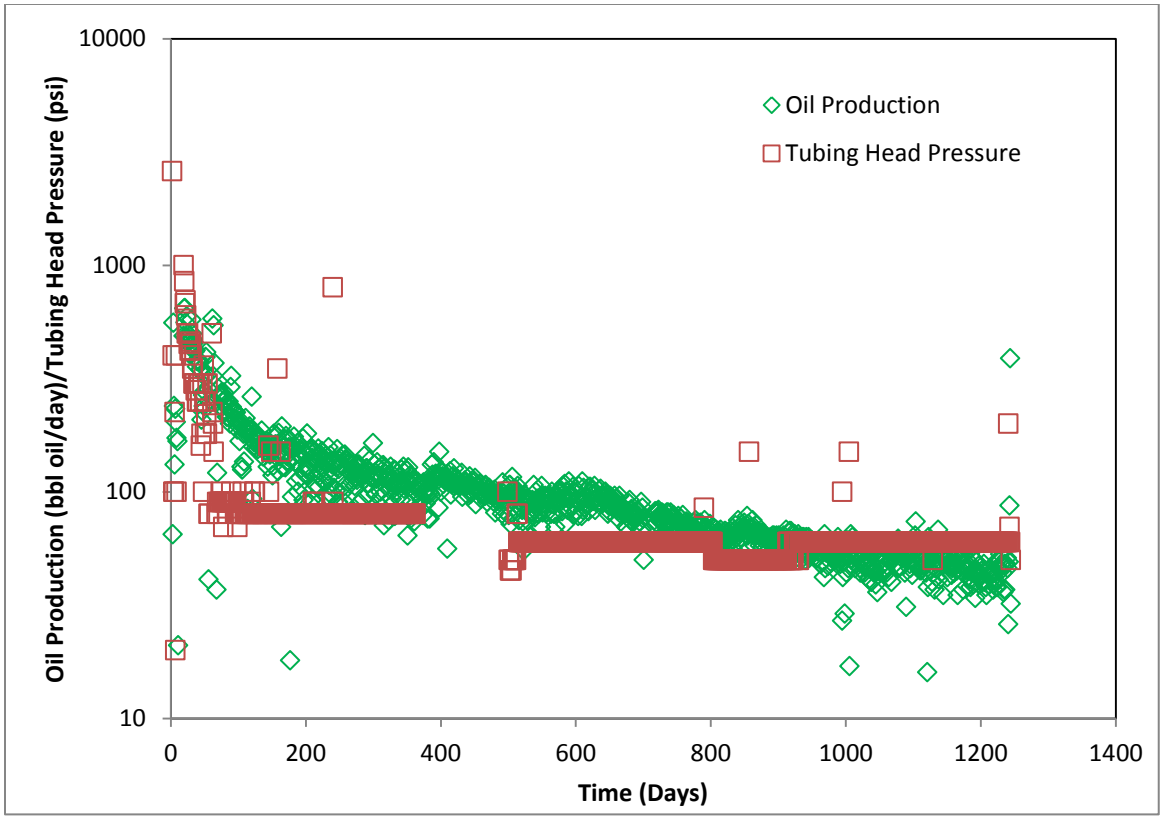

Figure 14: Oil Production Rate (Log Scale) and Tubing Head Pressure (Log Scale) vs. Time (Linear Scale) From Well UTID: 4

From the observation of straight line sections in the oil production rate (log) vs. time (linear) plot and the observation of the straight line sections in the oil production (log) vs. cumulative production (linear) plot, it is plausible to think that this type of production can be modeled as two or more tanks producing one after another; these two observations are very important to the development of the series model which is discussed further in chapter 4.

CHAPTER 4: 1-D SIMULATOR

4.1 Overview

A Microsoft Excel® based 1-D flow simulator with 11 serial cells was used to model shale oil production from fractured unconventional shale formations. The simulator has 11 cells that are coupled and connected in series described in Figure 15.

$$Well\ Rate = J(P_{cell\ 1} - P_{wf})$$

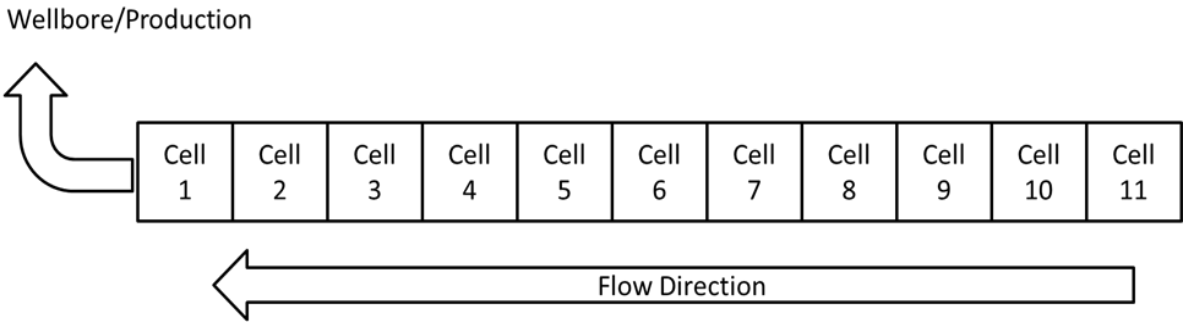

Figure 15: 1-D Simulator Organization

Cell 1 is where the well meets the cells and thus the flow flows from Cell 11 to Cell 1. Each cell contains the information on the following variables:

- Pore volume and its components: Δx [m], Δy [m], Δz [m]
- Transmissibility and its components: Δx [m], Δy [m], Δz [m], viscosity [cp], and permeability [md]
- Average pressure of current and previous time step in each cell

Global variables that were shared among all the cells or applied to the well were the following variables:

- Initial formation pressure [psia]

- Fluid viscosity [cp]
- Total compressibility [GPa^{-1}]
- Well pressure (the well was assumed to have constant pressure) [psia]
- Initial production productivity index [bbl/day-psi]

Engineering assumptions used in this model include the following variables:

- Only the oil phase is flowing
- Constant water oil ratio (WOR)
- Slightly compressible oil
- The systems are homogeneous enough where entire system (i.e. fractures, stimulated zones, matrix) properties can be summarized in one cell per system
- The bottom hole pressure is the static head of oil
- Although these wells are horizontal wells, single values of depths and pressures can describe the system

Furthermore, the time step that was used was one day.

For this study, the pore volume and transmissibility of each cell were the fitting parameters that were used to fit the model to the data. The well pressure and initial production productivity index were calculated from engineering assumptions. The well productivity index (J) can be a fitting parameter, but in this study, J was calculated to keep fitting parameters within the cell variables. The assumptions for initial pressure, fluid viscosity, and total compressibility were established through a meeting with the producer. A more detailed method is provided in Section 4.2.

The greatest strengths of this 1-D simulator are that it is easy to use and runs quickly. The run time is typically on the order of seconds and the optimizer time using the solver add-in function using a computer with dual 2.67GHz CPU and 4Gb RAM is less than 5 minutes. Also, the simulator uses physical properties that give estimations for pore volumes. Pore volume estimations cannot be done with the fitting parameters of typical decline curve analysis(Arps, 1945).

4.2 How the 1-D Simulator Works

The simulator used in this study simulates one dimensional flow using 11 cell blocks which can have varying properties. Each cell is a tank and is connected to neighboring cells as in Figure 15. The equations that govern the simulator are discussed in this section.

The simulator numerically solves material balance for each of the cells at every time step. The material balance for slightly compressible oil is stated in the continuity equation stated in Equation 4.

$$V_p c_t \frac{d\bar{p}}{dt} = -q(t) \tag{4}$$

V_p is the pore volume, c_t is the total compressibility, $\frac{d\bar{p}}{dt}$ is the change in average pressure per change in time, and $-q(t)$ is the net in/out flow rate for a cell at a given time. The $V_p c_t \frac{d\bar{p}}{dt}$ term is the accumulation term and $-q(t)$ is the net rate (flow in-flow out). Equation 4 applies for single-phase flow in slight compressible systems when the reservoir is viewed as a series tank (Lake, 2013).

To solve this problem, the system is defined as the cartoon in Figure 16.

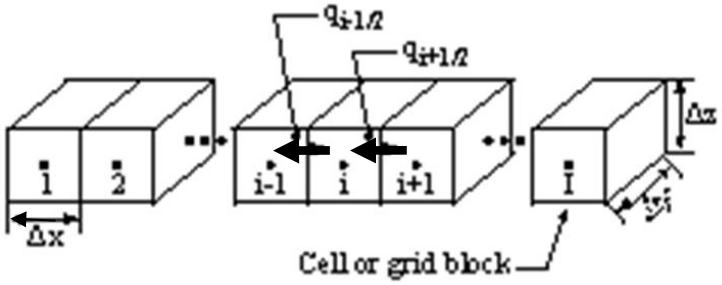

Figure 16: Labeled Cell Blocks of a 1-D Simulator (Lake, 2013)

In accordance with this system we can redefine the following:

- $\bar{p} \Rightarrow p_i$ Average pressure in cell i
- $V_p \Rightarrow \phi \Delta V_b$ ΔV_b is the bulk volume defined as: $V_b = \Delta x \Delta y \Delta z$
- $q \Rightarrow q_{interblock} + q_{wells}$ Where q_{wells} is the source term

With the above substitutions, Equation 4 becomes Equation 5.

$$\phi_i \Delta V_b c_t \frac{dp_i}{dt} = q_{interblock} + q_{wells} \tag{5}$$

The flow through the cell, $q_{interblock}$, can be visualized as Figure 17.

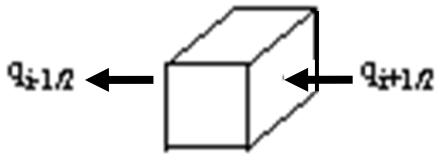

Figure 17: Flow Through an Individual Cell Visualized (Lake, 2013)

As such $q_{interblock}$ can be redefined as Equation 6.

$$q_{interblock} = q_{i+1/2} - q_{i-1/2} \tag{6}$$

Using Darcy's Law, $q_{i+1/2}$ and $q_{i-1/2}$ can be further broken down into Equation 7.

$$q_{i-1/2} = TI_{i-1/2}(p_{i-1} - p_i), q_{i+1/2} = TI_{i+1/2}(p_i - p_{i+1}) \tag{7}$$

TI is defined as the transmissibility. The transmissibility index is analogous to the productivity index, evaluated at the cell face, and determined from serial flow (Lake, 2013). Using this definition of transmissibility index and by substituting $\frac{dp_i}{dt}$ with $\frac{p_i^{n+1} - p_i^n}{\Delta t}$ (implicit procedure), Equation 4 becomes Equation 8.

$$\phi_i \Delta V_b c_t \frac{p_i^{n+1} - p_i^n}{\Delta t} = TI_{i-1/2}(p_{i-1}^{n+1} - p_i^{n+1}) - TI_{i+1/2}(p_i^{n+1} - p_{i+1}^{n+1}) + q_{wells} \qquad (8)$$

In Equation 8, the subscript *i* represents the i[th] cell block and the superscript *n* and *n+1* represents the time level (Lake, 2013). Time level is a concept to track the events of a previous time step (time level = *n*) and to mark the unknowns to be calculated (time level = *n+1*) (Lake, 2013).

Using the definition $T_{i-1/2} = TI_{i-1/2}\Delta t$ and $T_{i+1/2} = TI_{i+1/2}\Delta t$, Equation 8 can be written as Equation 9.

$$-T_{i-1/2} p_{i-1}^{n+1} + T_i p_i^{n+1} - T_{i+1/2} p_{i+1}^{n+1} = \phi_i \Delta V_b c_t p_i^n \qquad (9)$$

T is the transmissibility.

Solving Equation 9 would result in the knowledge of the flow in each block. To solve Equation 9, a matrix was used to calculate the relationship between the varying time levels were set up in an Excel spreadsheet to calculate pressures at each time step. The unknowns, the pressures in the next time level (time level = *n+1*), were solved for

using matrix inversion. Figure 18 shows how the solution was set up to solve for the unknowns.

$$\begin{bmatrix} T_1 & -T_{3/2} & 0 & 0 \\ -T_{3/2} & T_2 & -T_{5/2} & 0 \\ 0 & -T_{5/2} & T_3 & -T_{7/2} \\ 0 & 0 & -T_{7/2} & T_4 \end{bmatrix} \begin{pmatrix} p_1^{n+1} \\ p_2^{n+1} \\ p_3^{n+1} \\ p_4^{n+1} \end{pmatrix} = \Delta V_b c_t \begin{bmatrix} \phi_1 p_1^n \\ \phi_2 p_2^n \\ \phi_3 p_3^n \\ \phi_4 p_4^n \end{bmatrix}$$

Matrix Unknowns Forcing function

Figure 18: Sample Matrix Set Up for Simulator when i=4 (Lake, 2013)

The well was set up as a constant pressure boundary on the side of cell 1 that is not connected to cell 2. Fluids flowing out of the side of cell 1 that is not connected to cell 2 were considered to be the produced fluid. The well properties were governed by Equation 10.

$$q_{well} = q_k \qquad \text{where} \qquad q_k = J_k(p_{I_k} - p_{wf,k}) \tag{10}$$

J_k is the productivity index of well k and is defined by Equation 11.

$$J_k = \frac{2\pi(k_o)_{I_k}\Delta z}{\mu_o\left[\frac{1}{2}\ln\left[\frac{4\Delta x\Delta y}{\gamma C_{A,k} r_{w,k}^2}\right] + \frac{1}{4} + s_k\right]} \tag{11}$$

When the well properties are incorporated, the mass balance takes the form of Equation 12.

$$-T_{i-1/2}p_{i-1}^{n+1}+T_i p_i^{n+1}-T_{i+1/2}p_{i+1}^{n+1}=\phi_i \Delta V_b c_t p_i^n-\Delta t\delta_{iI_1}J_1\left(p_i^{n+1}-p_{wf,1}\right) \quad (12)$$

Where

$$\delta_{iI_k}=\begin{cases}1 & I_k=i\\ 0 & I_k\neq i\end{cases} \quad (13)$$

To solve Equation 12 linear algebra is used in the form of Figure 19. Figure 18 is assuming that the simulator has 4 cells, and the well is in cell 1.

$$\begin{bmatrix} T_1 & -T_{3/2} & 0 & 0\\ -T_{3/2} & T_2 & -T_{5/2} & 0\\ 0 & -T_{5/2} & T_3 & -T_{7/2}\\ 0 & 0 & -T_{7/2} & T_4 \end{bmatrix}\begin{pmatrix} p_1^{n+1}\\ p_2^{n+1}\\ p_3^{n+1}\\ p_4^{n+1}\end{pmatrix}=\Delta V_b c_t\begin{bmatrix}\phi_1 p_1^n\\ \phi_2 p_2^n\\ \phi_3 p_3^n\\ \phi_4 p_4^n\end{bmatrix}-\begin{bmatrix}\Delta t q_1\\ 0\\ 0\\ 0\end{bmatrix}$$

Figure 19: Sample Matrix for Simulator Set Up Including Well Term When n=4, k=1 (Lake, 2013)

Solving $q_k=J_k(p_{I_k}-p_{wf,k})$ (Equation 10) using the average pressure at the cell with the bottom hole pressure will result in the flow rate at the well.

4.3 Method of History Matching Using the 1-D Simulator

1. Develop a conceptual model of the simulation – An initial rough estimation of the pore volume and expected permeability should be developed.
2. Create data - The data originated in the form of a relational database. A query was used to match the correct well summary data to the appropriate production data.
    a. Run query.
    b. Export data to be used.
3. Import data to the simulator. Visual Basic for Applications (VBA) code was used to:
    a. Efficiently copy the correct data onto the simulator template
    b. Save the resultant workbook as a new file with the well code as the workbook name.
4. Enter the given variables.
    a. Initial pressure.
    b. Fluid viscosity.
    c. Total compressibility – was always assumed to be 1.45 GPa^{-1}. This value is consistent with the compressibility value used by Tran et al. (2011) to simulate the Bakken formation; Tran et al. used 1.7GPa^{-1}.
    d. Well depth.
    e. True vertical thickness of the formation.
5. Calculate and enter the calculated variables.
    a. Producing bottom hole pressure (pressure at the bottom of the well)- is calculated because the producing bottom hole pressure is needed to establish the pressure gradient that controls the flow. The producing bottom hole pressure was

considered to be constant from the observation of the tubing head pressure staying constant.

i. Calculate the bottom hole pressure as the static head of oil from the surface:

$$P_{wf} = \rho_{oil} g h \quad (14)$$

P_{wf} is the bottom hole pressure, ρ_{oil} is the density of oil, g is the acceleration from gravity, and h is the depth to the formation. $\rho_{oil}$was assumed to be 0.8 * ρ_{water}. This value was determined through a meeting with the producer.

ii. Enter the bottom hole pressure.

b. Initial well productivity index – is calculated as the initial productivity index provides insight to the initial producing conditions.

i. Select the largest oil production value in the first 30 days of production to be q_i.

ii. Calculate productivity index using the relationship given in Equation 15:

$$J_i = q_i / (p_{1,i} - p_{wf}) \quad (15)$$

q_i is the initial production (selected in step i), $P_{1,i}$ is the average initial pressure and P_{wf} is the bottom hole pressure.

6. Input an initial generic pore volume and transmissibility for each cell - These values should be from the conceptual model.
7. Conduct an "eyeball" fit of the data. The data would be manually adjusted with until the objective function was close enough for the Solver add-in to work. When using R^2 to measure the "goodness" of fit, the "eyeball" fit was considered to be done when the R^2

value was positive; the objective function was looking for how close the absolute value of the R^2 value was to 1 and any negativeR^2 values would result in the solver add in trying to make R^2 equal to -1.

8. Run the solver add-in.
    a. Select the appropriate objective function. The objective function when using R^2, to measure the goodness of fit is given in Equation 16.

$$\boldsymbol{Obj = \left|1 - \left|R^2\right|\right|} \quad (16)$$

This function was chosen because when the objective function approaches 0, R^2 should approach 1 (a perfect fit). A weakness is that R^2 must be positive before this objective function is effective.

    b. Select all of the cells to be guessed.
    c. Run solver add-in.
9. Check if the model fits the data. Judgment is exercised in this step. The solver add-in can have problems; some common problems were that the solution included non-physical values for variables, the "eyeball" fit captures the flow regimes better (resulting from only looking to minimize the objective function), and solver add-in failing to converge on a solution.
    a. Check if all the variables are physical and consistent with the conceptual model.
    b. Check if the flow regimes are captured in the simulated results.
10. Repeat steps 6-8 until the desired fit is obtained. Typically a desired fit is a model with a R^2 value greater than 0.5)
11. Gather collective data of all the fits and conduct analysis.

Figure 20 is a screen shot of a simulation run where the data was fit using the 1-D simulator with this method. It is showing the data entry portions and the simulation results plotted with the production data.

Well No.	**4**										
i=	1	2	3	4	5	6	7	8	9	10	11
Pore Volume	55883.73	87532.75	100162.38	931999.23	100.00	100.00	100.00	100.00	100.00	100.00	100.00
Transmissability	500	100	25.0454647	10	0.001	0.001	0.001	0.001	0.001	0.001	0.001
PI	Well rate	Well pressure	initial pressure		depth	hydrostatic	TVT		Viscosity		
bbl/psi-day	bbl/day	psia	psi	Mpa	ft	psi	ft	m	cP		
0.24	2000.00	3398.75	6114.36	42.16	9811.64	3398.75	47.53	14.49	0.50		

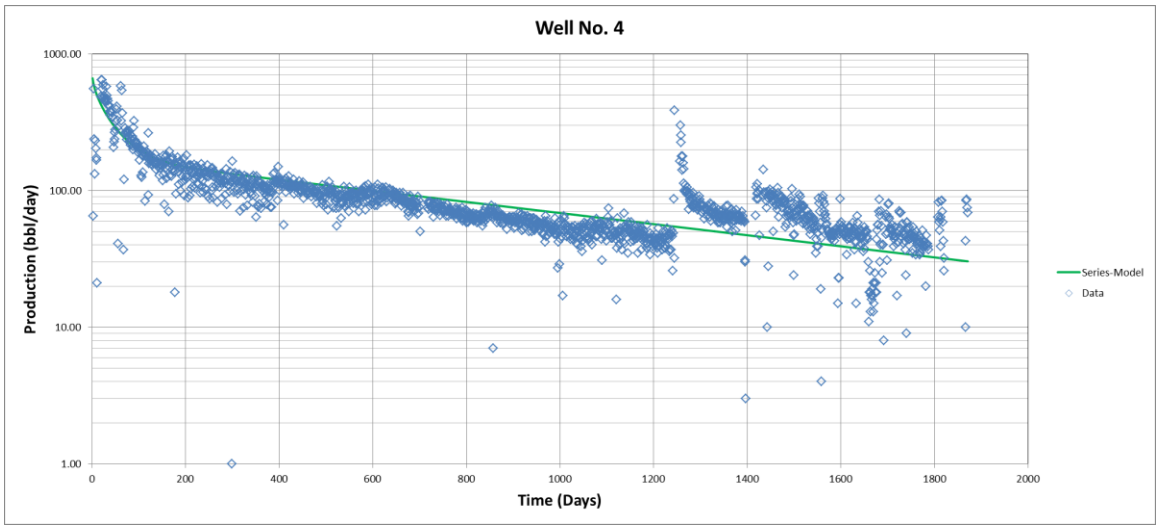

Figure 20: Screenshot of a Simulation Run where the Data was Modeled Using the 1-D Simulator

CHAPTER 5: PRE-MODELING SIMULATOR SENSATIVITY STUDY

5.1 Overview

Before the organized 4-Cell model runs, the 1-D simulator was used to fit the daily production data. The pre-modeling simulator sensitivity study was done to gain an understanding of how the simulator works and to confirm that the 1-D simulator can fit the data. In the pre-modeling study, the effects of perturbations to base cases were studied.

The main differences between the pre-modeling study and the organized 4-Cell model are:

- The 4-Cell model has a conceptual model, but the pre-modeling study does not. The pre-molding study is more of a exercise to get familiar with the 1-D simulator.
- The fitting parameters that are used for the pre-modeling study are the permeability, Δx, Δy, and Δz. In the 4-Cell model, the variables that are used for fitting parameters are the pore volume and transmissibility.

5.2 Pre-modeling Simulator Sensitivity Study Method

The following describes the study method:

1. Select the 62 wells with the production data that has the fewest "jumps"
2. Import data to the simulator
3. Manually adjust the permeability, Δx, Δy, and Δz of each cell until the objective function or the R^2 is acceptable. More discussion on the objective functions are in Section 5.3.2)
4. Run solver add-in (using permeability, Δx, Δy, and Δz as the adjusted fitting parameters)
5. Observe results and make conclusions

5.3 Pre-modeling Simulator Sensitivity Study Results

Production data from 62 wells were fit with the 1-D simulator. As such, not all of the results are shown in this thesis. The results that are shown in this thesis are:

- Example of a production data fit with the 1-D simulator
- Discussion about fitting with all 11 cells vs. 4 cells.
- Example of multiple simulations with different permeability, Δx, Δy, and Δz fitting the same well production data (demonstrating non-uniqueness of the solutions).

During this study, different objective functions were used to find the best objective function for the 1-D simulations. The objective function is mentioned by each figure.

5.3.1 Example of a production data fit with the 1-D simulator

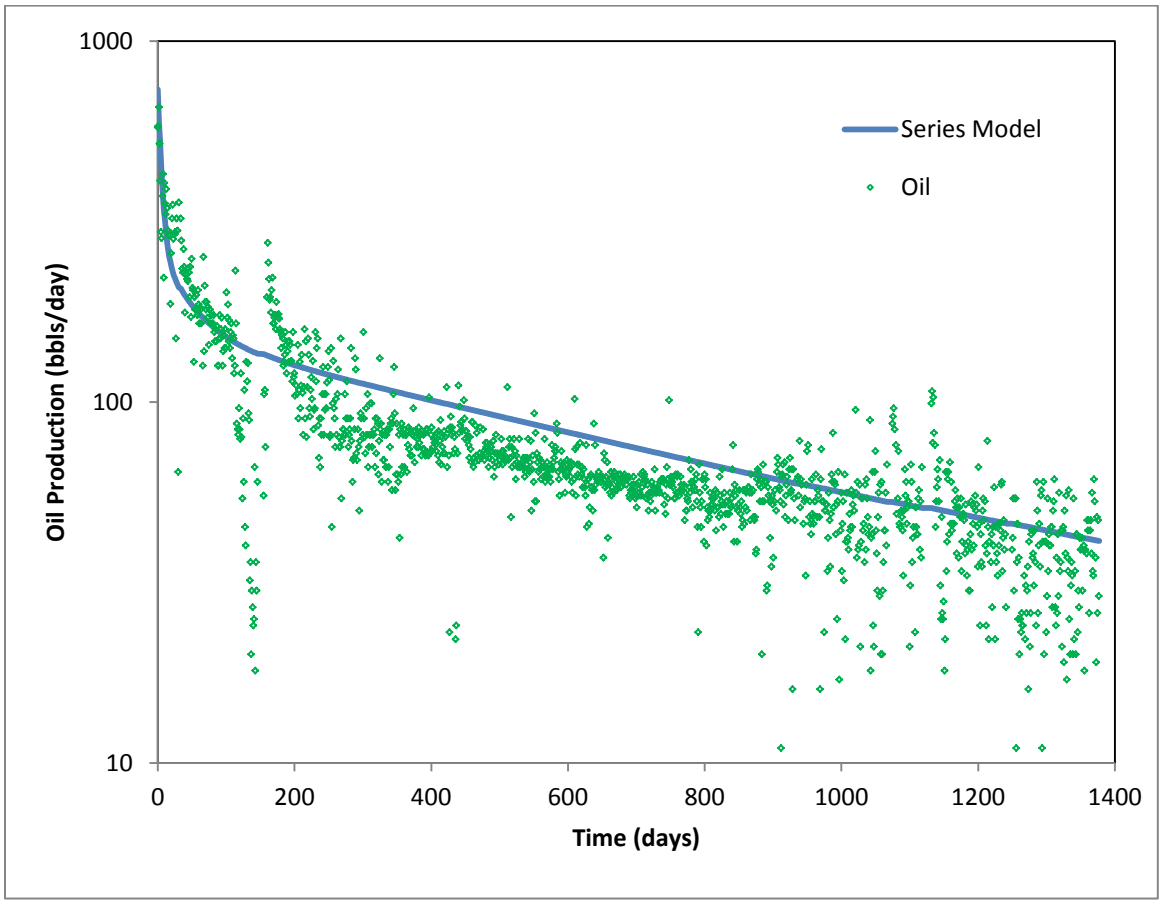

Figure 21: Oil Production vs Time Data Fit Using 1-D Simulator with R^2 as Objective Function From Well UTID: 197

Figure 21is an example of a production data fit with the 1-D simulator using R^2 as the objective function. The R^2 of the series simulation was 0.79. The simulator simulates the fast-early decline (from the start of production to approximately 150 days) and the slow-late decline (after approximately 200 days). The series simulation is inside the scatter of data for most of the data. The simulation is the result of the variables in Table 6.

Table 6: Simulation Variables for Results in Figure 21(From Well UTID: 197)

Cell	1	2	3	4
Δx, m=	183.77	211.71	431.21	643.09
Δy, m=	183.77	211.71	431.21	643.09
Δz, m	21.52	21.52	21.52	21.52
porosity, fr=	0.07	0.07	0.07	0.07
k, md=	235.23	0.31	1.99	0.01
viscosity, mPa-s=	0.50	0.50	0.50	0.50
C_t, GPa^{-1}=	1.45	1.45	1.45	1.45
J, bbl/MPa-day	29.0			
BHP, psi	3612.128			
Initial Pressure, MPa	24.9			
Formation Depth, m	3178.3			

Table 6 lists the different permeability (k), Δx, Δy, and Δz variables used to fit the simulation in Figure 21. From cell to cell, different values were used for permeability, Δx, Δy, and Δz. Especially from cell 1 to cell 2, the permeability drops from 235.23md to 0.31md. This change in scale is responsible for the different flow regimes.

5.3.2 Discussion about fitting with all 11 cells vs. 4 cells

There are eleven cells in the simulator, but at most 4 cells were altered when the solver add-in was used to adjust the cell variables. To confirm that only 4 cells were needed to simulate the production data, variables in cells 1~11 were set to be altered after variables in cells 1~4 have already been set.

There was negligible difference when the Solver add-in was used to fit the 1-D simulation solution to the production data using all 11 cells versus just using 4 cells. In the majority of the comparisons, there was no difference. Table 7 tracks the changes in

the variable Δx (the variable that saw the greatest change) between the simulation using 11 cells versus 4 cells.

Table 7: Changes in Δx between Simulation Using All 11 Cells vs. 4 Cells (From Well UTID: 691)

	i=	1	2	3	4	5	6
11 Cell	Δx, m=	2.01E+02	1.47E+02	1.71E+02	5.42E+01	1.00E+02	1.00E+02
4 Cell	Δx, m=	2.01E+02	1.47E+02	1.71E+02	5.42E+01	1.00E+02	1.00E+02
Change	Δx, m=	1.00E-02	1.00E-02	0.00E+00	0.00E+00	0.00E+00	0.00E+00

	i=	7	8	9	10	11
11 Cell	Δx, m=	1.00E+02	1.00E+02	1.00E+02	1.00E+02	1.00E+02
4 Cell	Δx, m=	1.00E+02	1.00E+02	1.00E+02	1.00E+02	1.00E+02
Change	Δx, m=	0.00E+00	0.00E+00	0.00E+00	0.00E+00	0.00E+00

The simulation results showed negligible sensitivity to changes in cells with i values greater than 4. When the simulation is optimized with the Solver add-in using all 11 cells or just the first 4 cells, the difference between the fitting parameters belonging to the 4 cell fittings and the 11 cell fittings were all less than 0.01% of each other.

The objective function described by Equation 17 was used for the 1-D simulations needed for the comparison between setting the solver add-in to change the variables in all 11 cells versus just the 4 cells closest to the well. The variables that were solved for using the solver add-in were the permeability, Δx, Δy, and Δz.

5.3.3 Example of multiple simulations with different permeability, Δx, Δy, and Δz fitting the same well production data

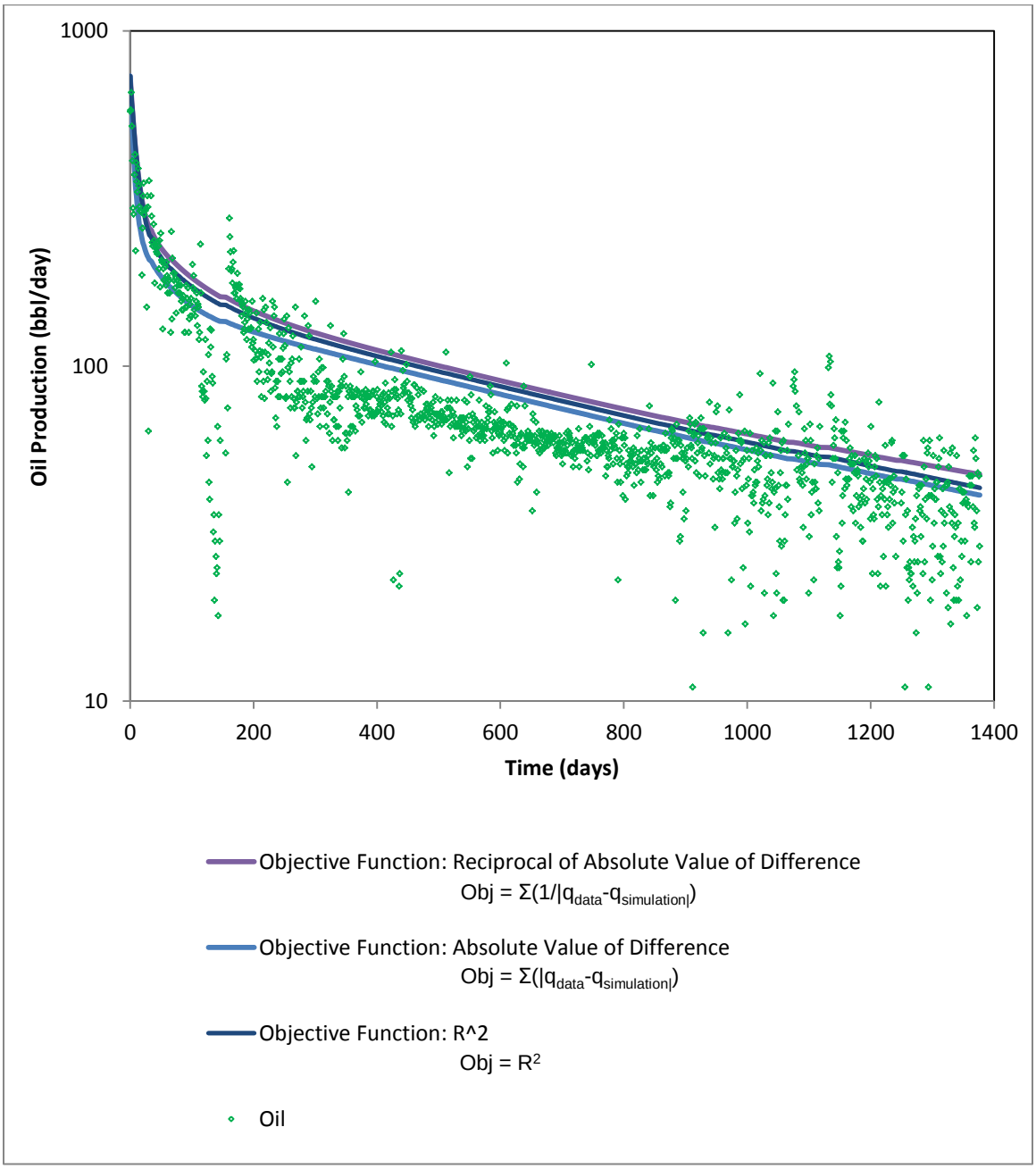

Figure 22: Oil Production vs Time Data Fit Using 1-D Simulator with Varying Objective Functions From Well UTID: 197

Figure 22 is the result of the same oil production data from well UTID: 197 simulated with the 1-D simulator using three different objective functions. The objective functions were defined as:

- The reciprocal of absolute value of difference

$$\boldsymbol{ObjectiveFunction} = \sum \frac{\mathbf{1}}{|q_{data,i} - q_{simulated,i}|} \quad (17)$$

  This objective function was set to be maximized in the solver add-in. This objective function resulted in a high chance of solver add-in converging. However the simulations that were fit using Equation 17 often had odd fits at small flow rates.

- The absolute value of difference

$$\boldsymbol{ObjectiveFunction} = \sum \left| q_{data,i} - q_{simulated,i} \right| \quad (18)$$

  This objective function was set to be minimized in the solver add-in. Equation 18 generally resulted in large objective function values (because flow rates at the start of production can be very large, and if the simulate did not match the data extremely well, this resulted in large error values). The large objective function values often resulted in the solver failing to converge or selecting non-physical variables (negative permeability, Δx, Δy, and Δz). When the data set was successfully fit using Equation 18, the solution often fit the high flow rate section of the curve well, but failed to match the lower flow rate sections. This is because fitting the high flow rate sections minimize the objective function much better than fitting the lower flow rate sections.

- R^2

$$\boldsymbol{R^2 = 1 - \frac{SS_{res}}{SS_{tot}}}$$

(19)

Where:

$$SS_{res} = \sum \left(q_{data,i} - q_{simulation,i}\right)^2$$

$$SS_{tot} = \sum \left(q_{data,i} - q_{averge,data}\right)^2$$

$$SS_{reg} = \sum \left(\log(q_{data,i}) - \log(q_{averge,data})\right)^2$$

R^2 was fit by minimizing Equation 16 which is based on R^2. When the simulation was adjusted manually until R^2 between 0 and 1, the chances of solver fine tuning the simulation was very high. Also, since the R^2 function compares the simulation solution to the average of the data flow rate, the resulting simulation solutions were better than the other two objective functions.

Figure 22 demonstrates that the same production dataset can have different simulation results based on the objective function used to simulate the data. R^2 was chosen as the objective function of choice because it is widely known/understood and it has a high chance of success when using solver add-in.

The ranges of R^2achieved in the models are further discussed in Chapters 7 and 8.

5.4 Conclusion

- The 1-D simulator can simulate production profiles that resemble the production data. Varying permeability and pore volume does create regions of different flow behavior.
- The objective function used for the solver fitting makes a difference.
- Four cells are enough to fit the simulator to the data. No more than 4 cells are needed.
- The solutions using the permeability, Δx, Δy, and Δz are not unique; meaning the same curve can be fit with many different combinations of permeability, Δx, Δy, and Δz.
- Solver add-in is not guaranteed to converge every time (R^2 closest to 1 or a minimized objective function) each time. Sometimes the starting permeability, Δx, Δy, and Δz had to be adjusted multiple times get the desired fit.

CHAPTER 6: MODELINFORMATION

6.1 Overview

As discussed in Section 3.3, 146 sets of well production data were modeled with the 2, 3, and 4-Cell Models. For each well, the pore volume and the transmissibility are used as the fitting parameters; the initial formation pressure, fluid viscosity, and total compressibility are obtained from the well summary data; the flowing well pressure and the initial productivity index are calculated. Discussion regarding how these variables are used is in Chapter 4.

To limit the use of cells to 2, 3, and 4 cells out of a total of 11 cells, the effects of cells furthest away from the well that were not being used had to be minimized. This was achieved by giving each cell that is not in use a small pore volume and small transmissibility; rock transmissibility is defined as:

$$Rock\ Transmissibility = k\frac{\Delta y \Delta z}{\Delta x}$$

* The viscosity term was removed for rock transmissibility as fluid viscosity was assumed to be constant

The values that were given to the cells that were not being optimized were:

- Pore volume = 100 [m^3]
- Transmissibility * viscosity = Rock Transmissibility = 0.001[md*m]

Each model is based on the observations from the previous model; the results of this study are in Chapter 7. The conceptual models for the simple models are described in this chapter.

6.2 4-Cell Model

The 4-Cell model was the first of the series models developed to fit the production data. In this model, the transmissibility and pore volumes of only the four cells closest to the well were modified.

The conceptual model for the 4-Cell model is that the oil will originate in the shale rock, flow to a slightly stimulated volume, flow to highly stimulated volume, and then flow into the propped fractures/wellbore where it will be produced. The following describes the expectations for each of the cells:

- Cell 1 is associated with the fracture and the wellbore. This cell was expected to have the smallest pore volume value and the largest transmissibility.
- Cell 2 is associated with a highly stimulated volume. This cell was expected to have a greater pore volume value than cell 1, but the pore volume value compared to that of cells 3 and 4 were undetermined. The transmissibility was expected to be less than that of cell 1 but greater than those of cells 3 and 4.
- Cell 3 is associated with a slightly stimulated volume. This cell was expected to have a greater volume than cell 1, but the pore volume value of cell 3 compared to that of cells 2 and 4 was unknown. The transmissibility value was expected to be less those that of cells 1 and 2 but greater than that of cell 4.
- Cell 4 is associated with the unstimulated matrix rock. This cell was expected to have a greater volume than cell 1, but the pore volume value compared to that of

cell 2 and cell 3 were undetermined. Also, cell 4 was expected to have the smallest transmissibility value as this is unstimulated rock.

6.3 2-Cell Model

The 2-Cell Model was developed to model the production data while mitigating the non-uniqueness of fits seen in the 4-Cell Model. In this model, the transmissibility and pore volumes of only the two cells closest to the well were modified.

The conceptual model for the 2-Cell model is that the oil will originate in the shale rock (unstimulated volume), then flow into fractured rock of varying transmissibility and produced (stimulated volume). Although the following relationships were not enforced, the following describes the expectations for each of the cells.

- Cell 1 is associated with the stimulated volume. This would include the well bore, propped fractures and the unpropped fractures. As we do not have geologic knowledge of how much volume is stimulated, there are no prediction was made about the pore volumes of Cell 1 compared to that of Cell 2. However as this is a stimulated volume, the transmissibility of cell 1 is predicted to be larger than that of cell 2.
- Cell 2 is associated with the matrix rock. Cell 2 is expected to have a smaller transmissibility than cell 1.

6.4 3-Cell Model

The 3-Cell model was the series models developed from physical estimations of pore volumes to fit the production data. In this model, the transmissibility and pore volumes of only the three cells closest to the well were modified.

The conceptual model for the 3-Cell model is that the oil will originate in the shale rock, flow to the stimulated volume, and flow into the propped fractures/wellbore where it is produced.

The approximations for pore volumes of each cell were based on Figure 23.

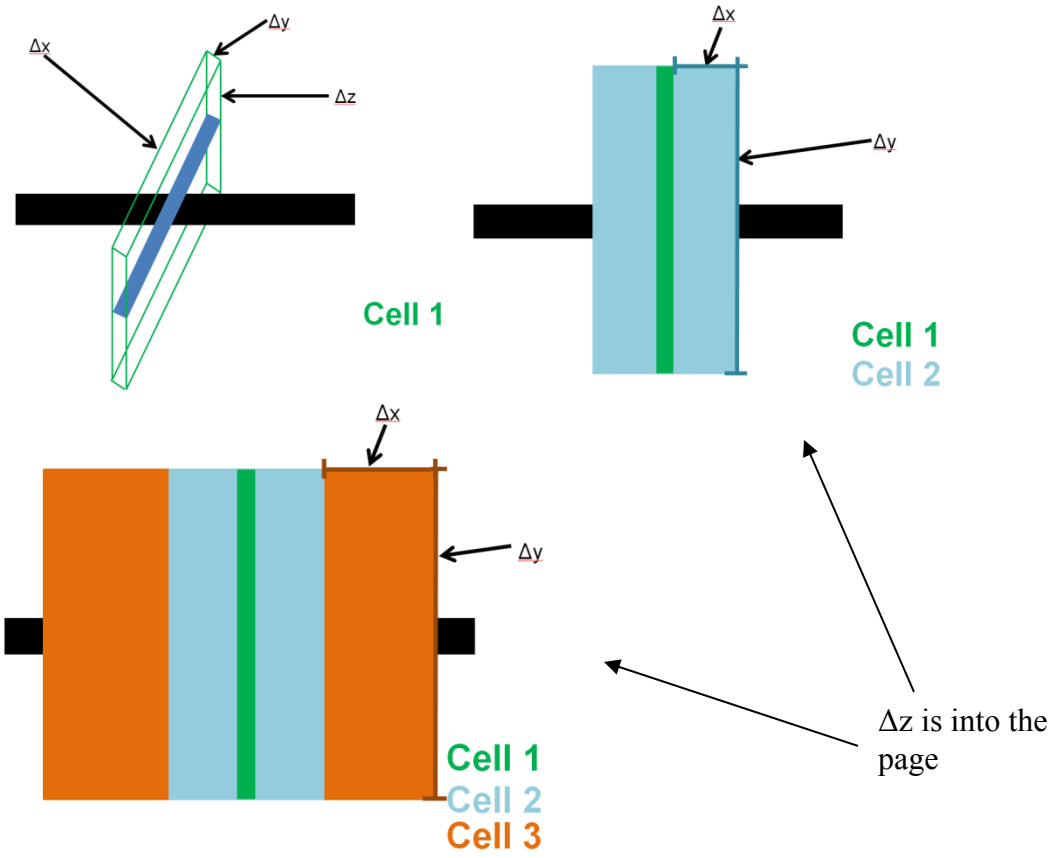

Figure 23: Conceptual Models for 3-Cell Model

- Cell 1 is associated with the fracture and the wellbore. As such, this cell should have the smallest pore volume value and the largest transmissibility.
- Cell 2 is associated with the stimulated volume. As such, this cell was expected to have a greater pore volume value than cell 1. The transmissibility was expected to be less than that of cell 1 but greater than those of cell 3.
- Cell 3 is associated with the unstimulated matrix rock. The transmissibility value was expected to be less those that of cell 1 and cell 2.

A set of assumptions, estimations for each pore volume, and the fitted pore volumes of a sample data set is in Table 8.

Table 8: Estimated 3-Cell Model Pore Volumes

From Well Summary	Avg TVT	15.24	m
	Init No. Stages	22	
	Lat Length	2931.66	m
Engineering Assumptions	Cell 1 Φ	0.3	
	Cell 2 Φ	0.07	
	Cell 3 Φ	0.07	
	Cell 4 Φ	0.07	
	Frac Length	200	m
	Frac Width	0.005	
	Stimulated Width	40	m
	cell 3 addition	50	m
	cell 4 addition	50	m
Calculated Approximate PV's	PV1	2.01E+02	m^3
	PV2	3.75E+05	m^3
	PV3	8.75E+05	m^3
Fitted PV's (UTID: 4)	PV1	2.00E+02	m^3
	PV2	2.75E+05	m^3
	PV3	1.03E+06	m^3

6.4.1 3-Cell Model without cell 1

The 3-Cell Models were compared to 3-Cell Models without cell 1 to see the effect of cell 1. The 3-Cell Models without cell 1 is essentially a 2-Cell model where cell 1 and has the same pore volume and transmissibility values of cell 2 cell 3 in the original 3 cell model respectively.

Cell 1 had values of pore volume at around 200 m^3 where the other cells have pore volume values that are over 100x greater than that of cell 1. From this observation, a hypothesis was developed that a cell 1 with a high transmissibility and small pore volume may not significantly affect the simulation results. The 3-Cell Models without cell 1 tested this theory.

The conceptual model is a shifted version the 3-Cell Model's conceptual model. Cell 1 would be representative the stimulated volume outside the propped fractures and cell 2 would be representative of the matrix rock.

The 3-Cell model without cell 1 assumes that the oil is produced when the fluid reaches the propped fractures. As such, it is like assuming that the propped fractures have infinite transmissibility.

CHAPTER 7: RESULTS

7.1 Overview

The results of this study are consolidated in this section. Section 7.2 demonstrates the models fitted to the production data. Section 7.3 discusses the R^2 obtained from the models. Section 7.4 discusses the issue of non-uniqueness in the 4-Cell Model. Section 7.5 discusses the effect of changing the R^2 from the R^2 of the flow rate to the R^2 of the log of the flow rate. Section 7.6 discusses the possible relationships between the model fitting parameters have with different variables.

The plots in section 7.6 are a subset of all the plots that were plotted to find relationships between the well summary data and the modeling results. All of the plots that were generated to find relationships are in Appendix B, C, and D.

7.2 Simulated Results

The series model fits for all of the models (4-Cell Model, 3-Cell Model, 2-Cell model, and the 3-Cell Model without cell 2) are consolidated in this section. Only the plots that illuminate information about the changing flow regime were plotted. Daily production data and models from well UTID: 4 were chosen to be plotted as it is representative of the daily production data; well UTID: 4 had regions demonstrating smooth decline behavior, a jump, and regions with scatter. The models are plotted in the following plots:

- Oil Production Rate (Log Scale) vs. Time (Linear Scale)
- Oil Production Rate (Log Scale) vs. Cumulative Oil Production (Linear Scale)
- Reciprocal Oil Production Rate (Log Scale) vs. Time (Log Scale)

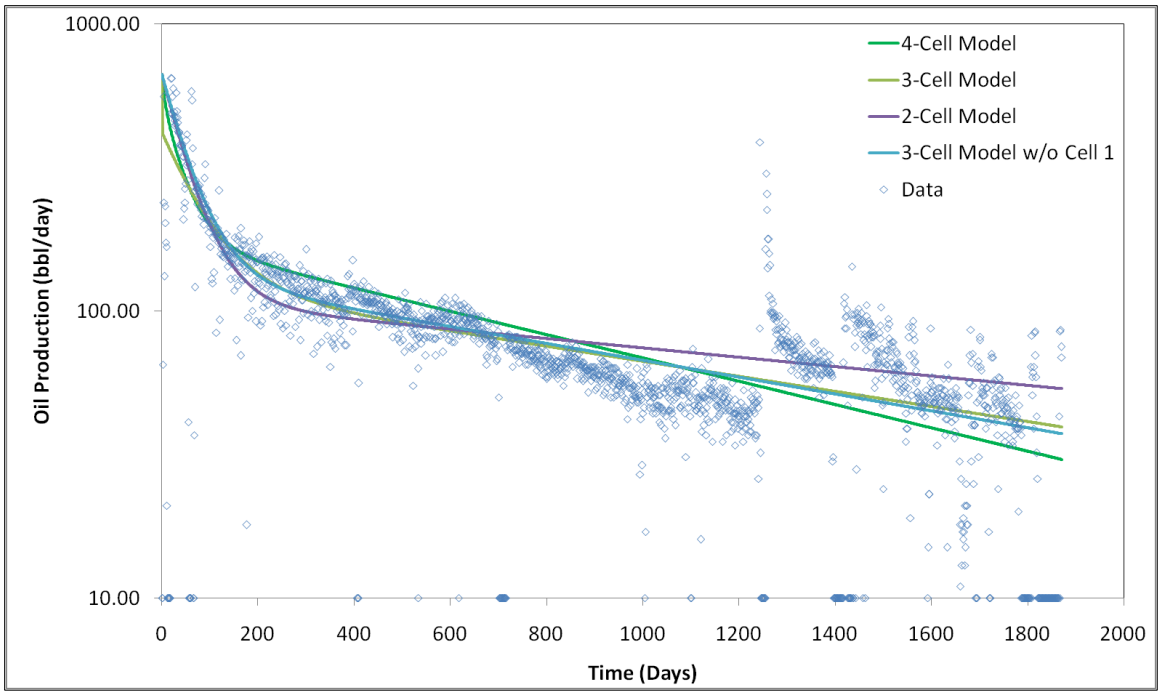

Figure 24: All Models Fitted to Oil Production Rate (Log Scale) vs. Time (Linear Scale) From Well UTID: 4

All of the models were able to consistently fit the production data. The models are able to capture the first flow regime change which occurs at approximately 150 days of production; the models match both the fast decline rates before 150 days and slow decline rates after 150 days.

The jump in the data at approximately 1300 days and the scatter in the data in the late time cause the models to diverge in the late times.

The 3-Cell Model and the 3-Cell Model without cell 1 appear very similar; cell 1 does contributes little to the late time flow behavior of the 3-Cell Model as it has a small pore volume and high permeability. The 2-Cell Model results in two linear sections in the oil production rate (log scale) vs. time (linear scale) plot. The 4-Cell model often

produced results that were not unique; the issue of non-uniqueness of the 4-Cell Model is discussed in Section 7.3.

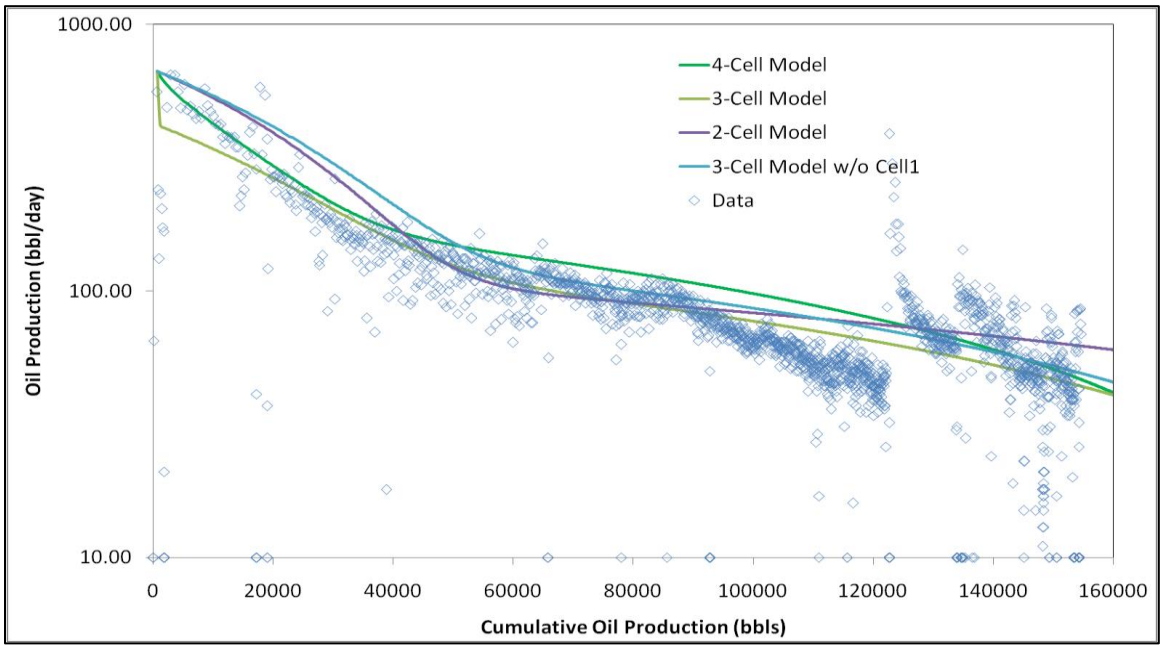

Figure 25: All Models Fitted to Oil Production Rate (Log Scale) vs. Cumulative Oil Production (Linear Scale) From Well UTID: 4

In Figure 25 the same models from Figure 24is plotted on an oil production rate (log scale) vs. cumulative oil production (linear scale).

In the 3-Cell Model, the effect of cell 1, which models the fracture volume, is accentuated in Figure 25. At the start of production, the 3-Cell Model experiences a more vertical drop in oil production where none of the other models do.

The data from these wells often seem like there are two straight line sections in the production rate (log scale) vs. cumulative oil production (linear scale) plots while the models are combined sets of downward sloping curves. The models are downward set of curves as the series model is tanks undergoing exponential decline connected in series. Although the difference in production may be small in the early time, the ultimate

recovery estimations may be conservative with the series model if the data continues to be linear at very late time.

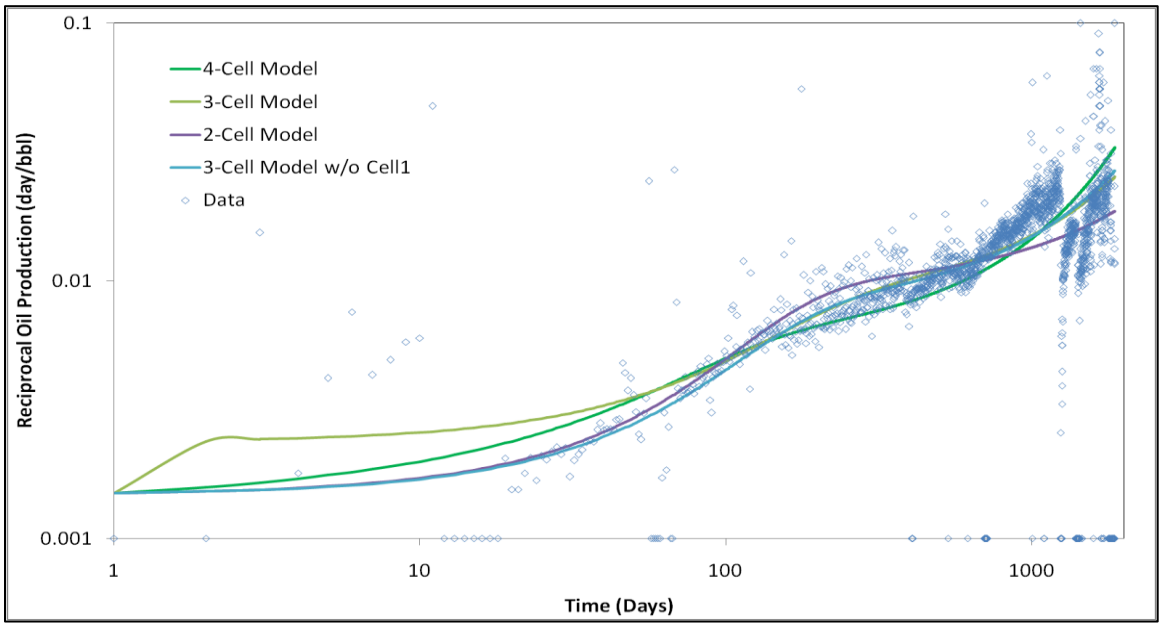

Figure 26: All Models Fitted to Reciprocal Oil Production Rate (Log Scale) vs. Time (Log Scale) From Well UTID: 4

In Figure 26 the same models from Figure 24 are plotted on a reciprocal oil production rate (log scale) vs. time (log scale).

The models again match the data well. Although the models are not straight line segments, the models bend and approximate the flow regimes.

The effect of cell 1 in the 3-Cell Model is seem in Figure 26 as the rapid rise of the reciprocal of oil production; meaning fast decline in oil rate. This rapid rise is not observed in data; it is likely that this rapid rise associated with the formation linear flow occurs too quickly to be seen in the data.

7.3 CDF of R^2

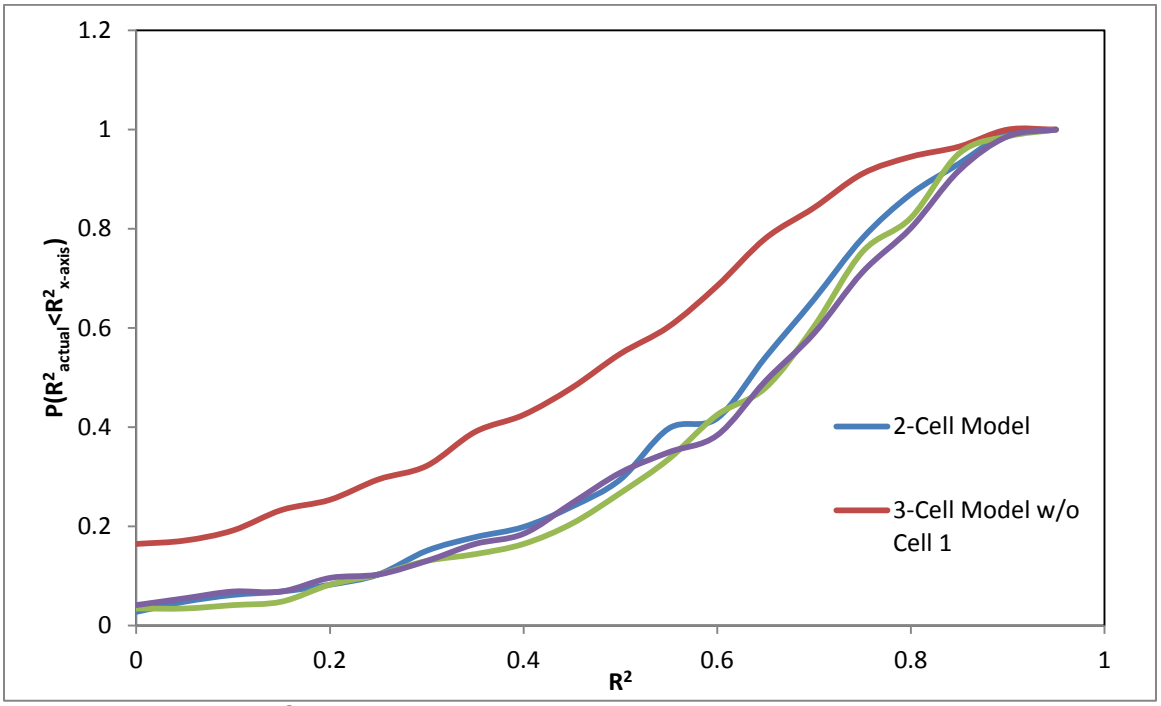

Figure 27: CDF of R^2 of All Models

As a whole, the models often have high R^2 values associated with good fit of the data. Over 60% of the models have R^2 values greater than 0.6 (not including the 3-Cell Model without cell 1). Also, the different models all have very similar R^2 values.

The 3-Cell Model without cell 1 had noticeably lower R^2 values as this was not a fitted model. However, the R^2 of the 3-Cell Model shows the importance of the cell 1 in the 3-Cell Model in terms of goodness of fit.

7.4 Non-uniqueness of the 4-Cell Model

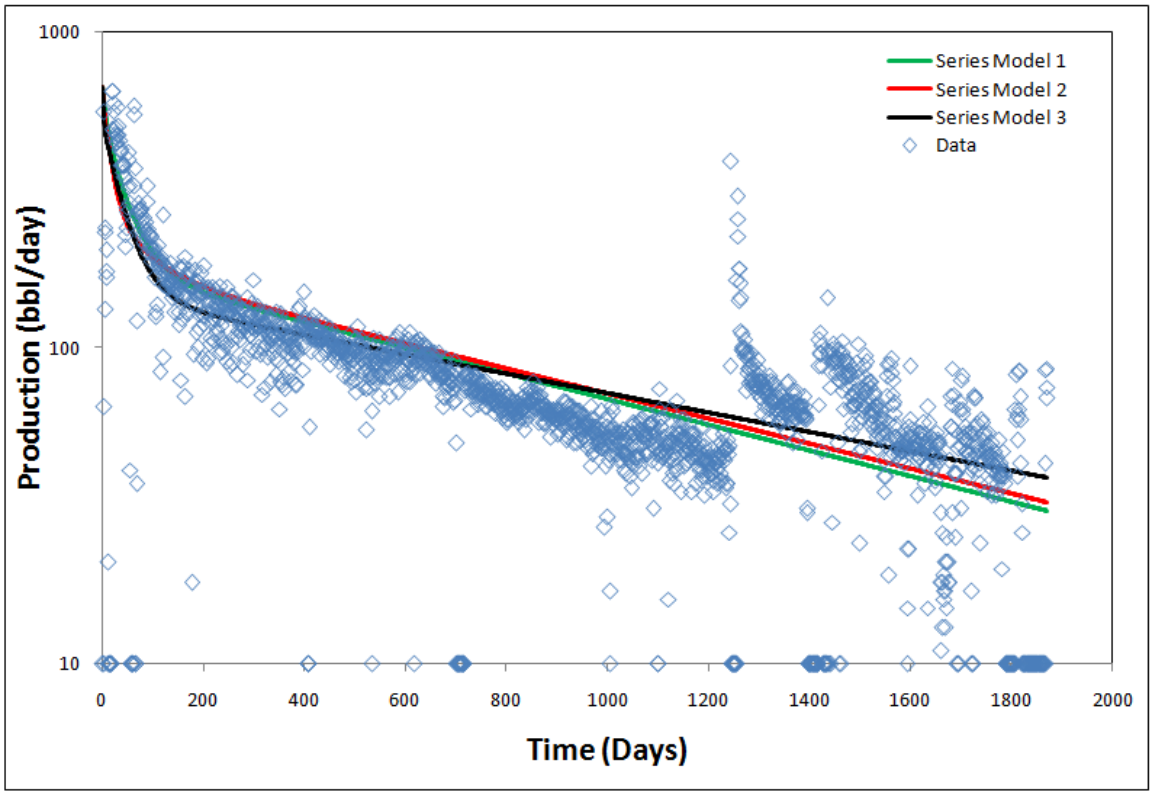

Figure 28: Three Different 4-Cell Models Fitted to the Data From Well UTID: 4

Table 9: Fitting Parameters used in Figure 28

	Series Model1		Series Model2		Series Model3	
	PV	Trans	PV	Trans	PV	Trans
Cell 1	55883.73	500.00	283.73	298189.00	20083.75	2000.00
Cell 2	87532.75	100.00	100532.75	227.68	150532.80	47.09
Cell 3	100162.38	25.05	300162.38	9.65	1162.41	20.52
Cell 4	931999.23	10.00	801998.98	501.62	1101998.98	10.00

The production data from well UTID: 4 was fitted with three different 4-Cell Models in Figure 28. All of the models are fitted with the Solver add-in but with different starting seed values. The non-unique nature of the 4-Cell Model is supported by Figure 28 as the model vales displayed in Table 9 are quite different from one another.

7.5 Sensitivity of Changing R^2 definition

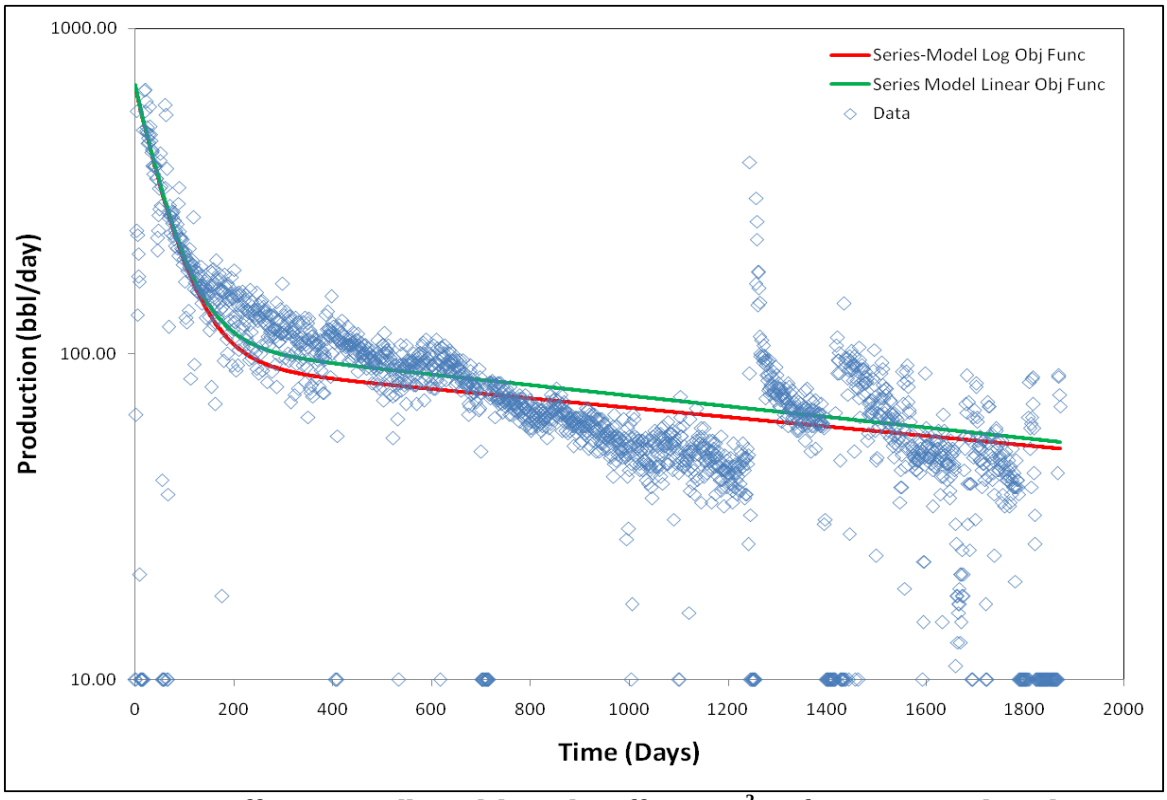

Figure 29: Two Different 3-Cell Models with Different R^2 Definitions Fitted to the Data From Well UTID: 4

A sensitivity study to see if changing the R^2 definition can enhance the model fits was conducted. Originally, the R^2 was taken from the difference of the flow rates; in this study, the R^2 was taken from the difference of the log of the flow rates. Although only the results from the 2-Cell Model is plotted in Figure 29,the 4-Cell Model, the 2-Cell Model, and the 3-Cell Model were all re-fitted with the changed definition of R^2.

There was not a big change when the R^2 definition was changed; most of the models had slightly lower flow rate when the new definition of R^2. However, solver add-in had a greater chance of success; this is likely because of the fact that the Solver was working with smaller numbers because of the log.

7.6 Variables showing relationships

The various fitted parameters and the calculated parameters of the 2, 3, and 4-Cell Models were plotted against well summary data variables find if relationships exist. This study focused on the 2-Cell Model and the 3-Cell Model as the solutions for the 4-Cell Model were not unique. Only the plots showing relationships are plotted in this section. See Appendix A for the complete set of modeled pore volume and transmissibility vs. productivity index and age of well, Appendix B for the modeled pore volume vs. various well summary data, and Appendix C for the modeled rock transmissibility vs. various well summary data.

The plotted fitted variables are:

- Pore volume
- Rock transmissibility

The plotted calculated variables are:

- Initial productivity index
- Age of well

The plotted well summary data variables are:

- Number of stages
- Lateral length
- Spacing
- Water cut
- Porosity
- Depth
- Overpressure
- Injection pressure
- Total fluid injected
- Mass of injected sand

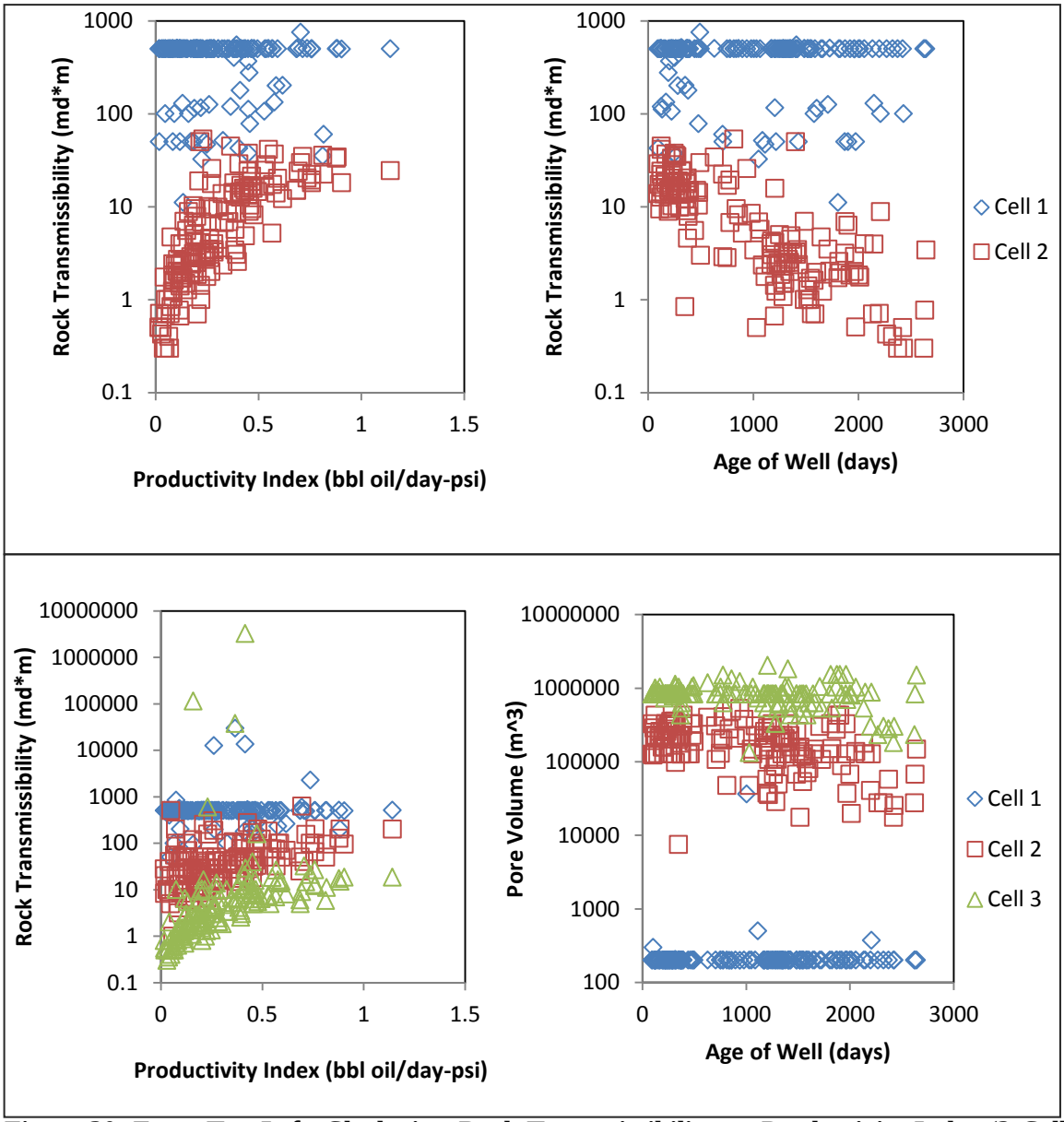

Figure 30: From Top Left, Clockwise: Rock Transmissibility vs. Productivity Index (2-Cell Model), Rock Transmissibility vs. Age of Well (2-Cell Model), Pore Volume vs. Age of Well (3-Cell Model), Pore Volume vs. Productivity Index (3-Cell Model)

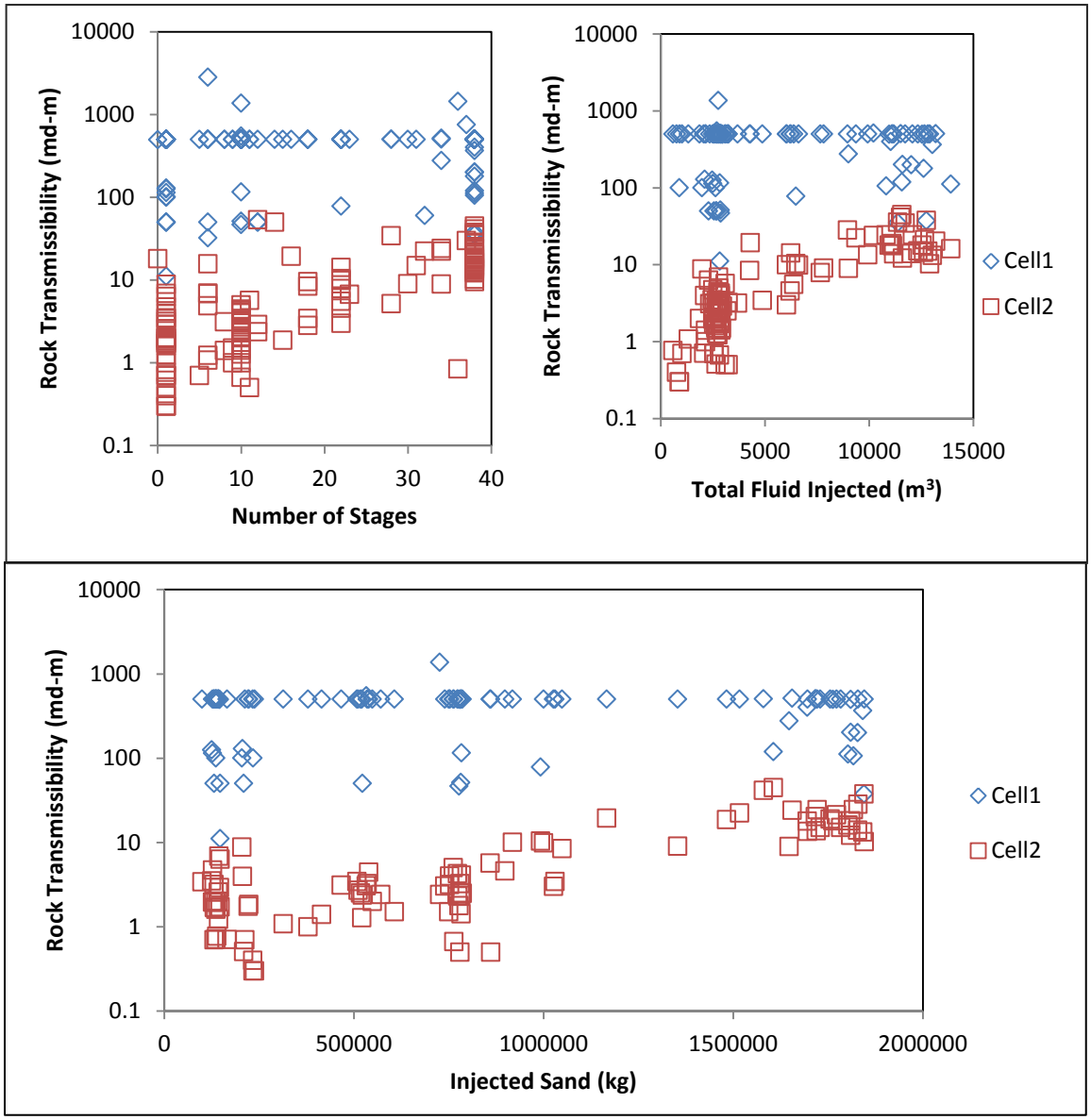

Figure 31: From Top Left,Clockwise: Rock Transmissibility vs. Number of Stages (2-Cell Model), Rock Transmissibility vs. Total Fluid Injected (2-Cell Model), Rock Transmissibility vs. Injected Sand (2-Cell Model)

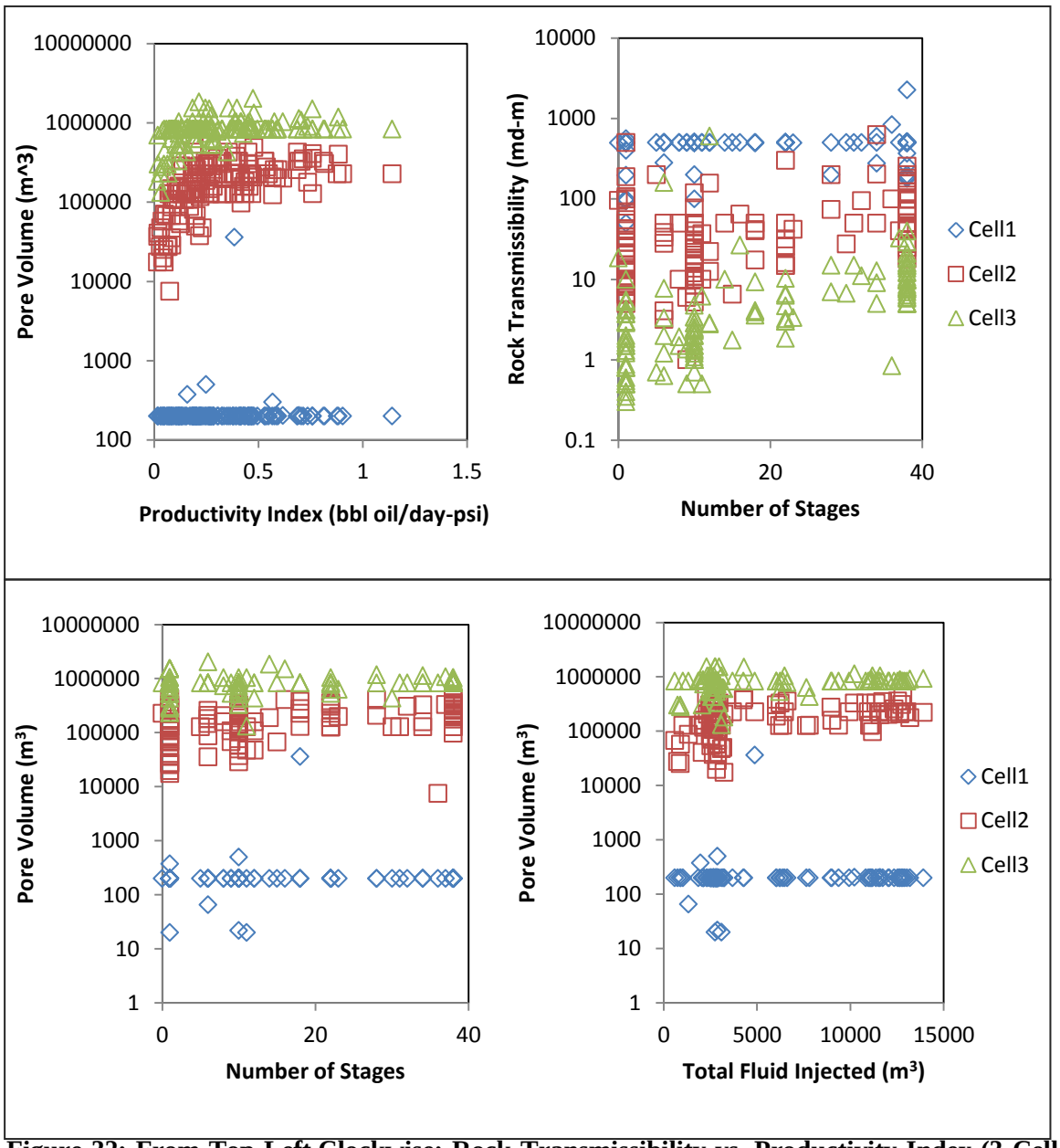

Figure 32: From Top Left,Clockwise: Rock Transmissibility vs. Productivity Index (3-Cell Model), Rock Transmissibility vs. Number of Stages (3-Cell Model), Pore Volume vs. Total Fluid Injected (3-Cell Model), Pore Volume vs. Number of Stages (3-Cell Model)

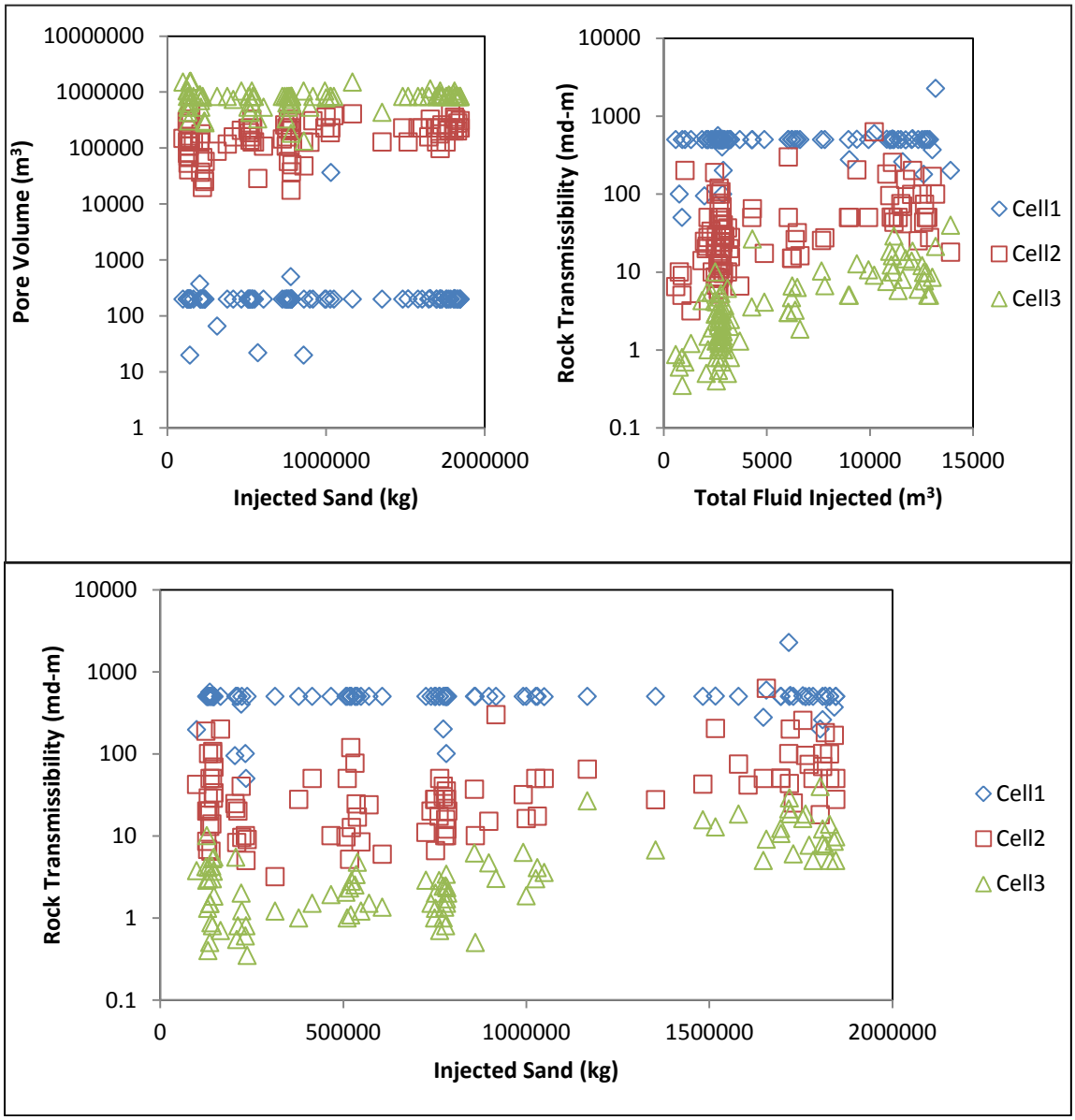

Figure 33: From Top Left, Clockwise: Pore Volume vs. Injected Sand (3-Cell Model), Rock Transmissibility vs. Total Fluid Injected (3-Cell Model), Rock Transmissibility vs. Injected Sand (3-Cell Model)

Figure 34: Initial Productivity Index vs. Length of Data (Age of Well)

- The rock transmissibility and the initial productivity index are positively related for cell 2 of the 2-Cell Model and cell 2 and 3 for the 3-Cell Model.
- The rock transmissibility and the age of well are negatively related for cell 2 of the 2-Cell Model.
- The pore volume of cell 2 of the 3-Cell Model is negatively related to age of well.
- The rock transmissibility is positively related to the number of stages, total fluid injected, and the injected sand for cell 2 of the 2-Cell Model.
- The pore volume is positively related to the productivity index, number of stages, and total fluid injected for cell 2 and cell 3 of the 3-Cell Model.
- The rock transmissibility is positively related to the number of stages for cell 2 and cell 3 of the 3-Cell Model.

- The pore volume is positively correlated to the injected sand in cell 2 of the 3-Cell Model.
- The rock transmissibility is positively correlated to the total fluid injected and the sand injected in cell 2 and cell 3 of the 3-Cell Model.
- Newer wells have a larger initial productivity index than compared to older wells.
- The 3 and 4-Cell Models are not sensitive to the changes in cell 1 as the final solutions do not change much from the initial seed value of roughly 200 m^3.

These relationships all suggest about quality of the stimulation of the wells. This set of relationships support the ideas:

1. Newer wells are more likely to have a more effective completion. This is seen in Figure 30 demonstrating the older wells have a smaller cell 2 pore volumes in the 3-Cell Models. It is also observed in Figure 34 demonstrating that the productivity indexes of newer wells are larger than that of old wells.
2. More effective frac-jobs increase the cross-sectional area of the stimulated volume. This would increase the pore volume and the transmissibility of the well. Evidence of this are seen in the positive relationships between the pore volumes and transmissibility compared to the number of stages, the total fluid injected, and the sand injected for both 2 and 3-Cell Models in Figures 31, Figure 32, and Figure 33.
3. There is a limit to how much adding stages, injecting more fluid, and injecting more sand will help the stimulation job. Positive relationship between the pore

volume and transmissibility compared to the number of stages, total fluid injected, and injected sand display a asymptotic relationship.

a) After approximately 20~25 stages, the number of stages does not increase the pore volume and transmissibility much.
b) After about 7000m^3 of fluid injected the rock transmissibility does not increase much.
c) After about 1000000kg of injected sand, the rock transmissibility does not increase much.

4. Cell 1 in both the 2 and 3-Cell Models are not sensitive in terms of pore volume and rock transmissibility. This is seen in the almost constant values of pore volume and rock transmissibility across the board.

CHAPTER 8: SUMMARY, CONCLUSIONS, AND FUTURE WORK

8.1 Summary

Daily production data, monthly production data, and well summary data from a fractured shale play were investigated in this study in order to use a simple model to describe such data. The simple model chosen to model oil flow from fractured shale formations was a Microsoft Excel® based 1-D implicit sequential finite difference flow simulator with 11 serial cells. The greatest strengths of this 1-D simulator are that it is easy to use and has a very short run time. Also, the simulator uses physical properties that give estimations for pore volumes. Pore volume estimations cannot be done with the fitting parameters of typical decline curve analysis(Arps, 1945).

The 1-D simulator was coupled with conceptual models to develop the 2-Cell Model, the 3-Cell Model, and the 4-Cell Model to fit 146 sets of daily production data from different wells.

The 4-Cell model was developed from the observation that only four cells were needed to simulate the production during the pre-modeling study. The 4-Cell model is able to fit production data well in terms of large R^2. The modeled production matched the production data well and matched the times when the flow regimes changed. However, the solutions to simulations done using the 4-Cell Model are not unique.

The 2-Cell model was developed to address the issue of non-unique solutions in the 4-Cell model. The 2-Cell model also fit the data well in terms of R^2. This model also

matched the time of the flow regime change well. However, there was no dedicated cell simulating the fracture in the 2-Cell Model.

The 3-Cell model was developed as a model based on physical estimations of the fracture and stimulated zone. This procedure made sense as the initial pore volume before solver add-in is estimated from realistic engineering guesses for the accessed pore volume. The 3-Cell model offered large R^2 values while matching the time when the flow regime changes. The 3-Cell Model is powerful as it accounts for the fracture in the modeling process; meaning if the model is calibrated further, fracture parameters (size dimensions, permeability, etc.) may be calculated from the simulation variables.

A side study was done on the 3-Cell model where cell 1, the cell representing the propped hydraulic fracture, was removed. This side study showed that representing the fracture is important to the 3-Cell Model results.

From the simulation results, relationships between the model parameters and the well summary data were found.

8.2 Conclusion

- All of the models fit the production data. They capture the different flow regimes to a degree. The series model is especially good at transitioning from the early-fast decline to late-slow decline
- Using just 1 cell does not fit the production data. When just 1 cell (1 tank) is used to model production, it only shows 1 flow regime in the log of production vs. log of time plot. This is demonstrated in Appendix E. At least 2 cells are needed to capture the different flow regimes.
- The models are not perfectly straight in the oil production rate (Log Scale) vs. cumulative oil production plots where the data appears to be straight. This is to be expected as a single tank flow model would result in an exponential decline (which does not have a straight line on the oil production rate (Log Scale) vs. cumulative oil production plot). This should not be a big problem when modeling fractured oil flow as the "bend" in the model at late time can be mitigated with a large cell pore volume with a small transmissibility.
- Changing the definition of R^2 from the R^2 of the flow rate to the R^2 of the log of the flow rate only alters the model slightly.
- Newer wells are more likely to have a more effective completion. This is seen in Figure 30 demonstrating the older wells have a smaller cell 2 pore volumes in the 3-Cell Models. Figure 34 demonstrates that the initial productivity indexes of newer wells are larger than that of old wells.

- More effective frac-jobs increase the cross-sectional area of the stimulated volume. This would increase the pore volume and the transmissibility of the well. Evidence of this are seen in the positive relationships between the pore volumes and transmissibility compared to the number of stages, the total fluid injected, and the amount of sand injected for both 2 and 3-Cell Models in Figures 31-33.
- Cell 1 in both the 2 and 3-Cell Models are not sensitive in terms of pore volume and rock transmissibility. This is seen in the almost constant values of pore volume and rock transmissibility across the board.
- The cell 1 which models the fracture volume causes the production rate to decline very rapid at the start of the production. This is evident when compared to other models. This rapid decline causes the 3-Cell Model to have a noticeably different production profile at early times.
- At late times the models did not match each other. This difference is likely because there is more data scatter at late time data.
- The 4-Cell Model simulates the production data well in terms of having fits with large R^2 values. However, it is unlikely that physical meaning can be extrapolated from the simulation results because of non-uniqueness of the solutions.
- The 2-Cell Model and the 3-Cell model simulate the production data well and are often unique. When the models are not unique, it is usually because there is a loss of sensitivity in one of the cells. Physical meaning may be extrapolated from the results of the 2-Cell Model and the 3-Cell Model in the future.

- The 2-Cell Model and the 3-Cell Model simulate the production data well and are often unique. The case when the models fail to be unique is loss of sensitivity when the transmissibility values are too high. Physical meaning may be extrapolated from the results of the 2-Cell Model and the 3-Cell Model in the future. The number of stages does not seem to change the rock transmissibility of the stimulated region in the 2-cell and 3-cell models after the number of stages exceeds about 20. Also there is no observed relationship between the number of stages and the pore volumes of the cells. From these observations, around 20 stages is the most cost effective way to complete a well in this setting.
- The total amount of fluid injected does not seem to increase the pore volume accessed or the transmissibility after approximately 7000m^3. Also, there is small positive correlation between the amount of sand injected and the pore volumes/transmissibility; after about 1000000kg of injected sand, the rock transmissibility does not increase much. One possible explanation for these trends is that the proppant (sand) is not effectively traveling down the hydraulic fractures; the proppant may be just dropping out near the well. This would result in parts of the fracture closing when production starts, and explain why the correlation between the fitting parameters and sand/fluid injected are low.

  From these observations, around 7000m^3 of fluid injected is the most cost effective way to complete a well in this setting. However if the proppant were moved further down the hydraulic fractures, the production pore volume may be greatly increased.

8.3 Future Work

1. The modeling of total fluid production, water production, and gas production. Only the production of oil was modeled in this work. However, there is water production (for all of the days) data and gas production data (for late time). The modeling of all the data should be attempted.

2. A re-modeling with more accurate bottom hole pressures. The bottom hole pressure in this study was assumed to be the hydrostatic head of oil. However, there is production of oil, water, and gas as well as a larger than atmospheric tubing head pressure. Using the all of the information and perhaps information about the production tubing, a more realistic bottom hole pressure can be calculated.

3. The production data from wells with different fracture designs should be obtained and modeled with the 3-Cell Model. The wells in this data set have very similar volume of fluid injected and mass of sand injected information. It would be informative to model and compare fluid production from wells from different fracture information.

4. Correlating cell 1 properties with fracture parameters should be attempted. This correlation would allow cell 1's variables to be calculated from the information from the well summary data.

5. A method of modeling the jumps (when the well is shut in then starts producing again) will allow the Series Model to model the data much more accurately. A study to

answer if the production after the well is reopened can be modeled by changing the cell pressures while keeping the rock properties is a good place to start.

6. The Series Model should be compared to other simple models. Babafemi Ogunyomi, a graduate student working for Dr. Larry W. Lake, is working on a simple model where the cells are connected in parallel (Parallel Model). This model is discussed in his doctoral dissertation to be completed in December 2014. It would be interesting to see the similarities and differences between the models.

7. There is well head coordinate information in the well summary data, but it could not be used for this study as the coordinate system was not reviled to us. If this coordinate system becomes clear, the effects of well location and proximity to other wells should be studied.

APPENDIX A

Comments

The graphs that were generated to find relationships between the well summary data and the model fitting parameters (transmissibility and pore volumes of each cell) are all plotted in Appendix B, C, and D; Appendix B plots the modeled pore volumes and transmissibility vs productivity index and age of well, Appendix C plots the modeled pore volumes vs. the various well summary data, and Appendix D plots the modeled transmissibility vs. the various well summary data. The plots showing relationships are discussed in Chapter 7 of the thesis.

Observations of the results

- Many of the transmissibility values seem very high. A possible explanation for this result is that the model loses sensitivity at large transmissibility values; when the transmissibility exceeds 100 md-m, changes in transmissibility effects the model very little.
- The cell 1 pore volume values do not seem to change much for the 3-Cell Model, and the 4-Cell Model. A possible explanation for this result is the loss of sensitivity of cell 1. Because the other cells are at least 100x larger than cell 1, changing the values of cell 1 may have negligible effect on the final model. So the Solver add-in may not have changed the pore volumes of cell 1 much from the seed value of 200 m^3.

APPENDIX: B

Modeled pore volume and transmissibility vs. productivity index and age of well

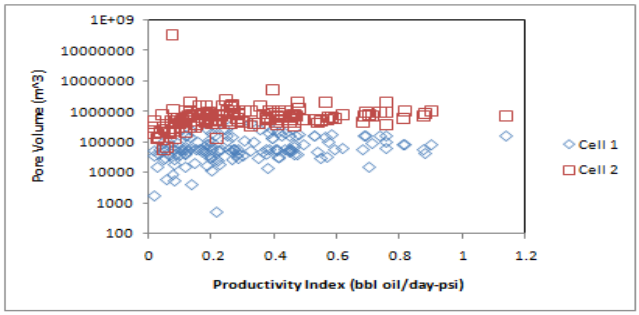

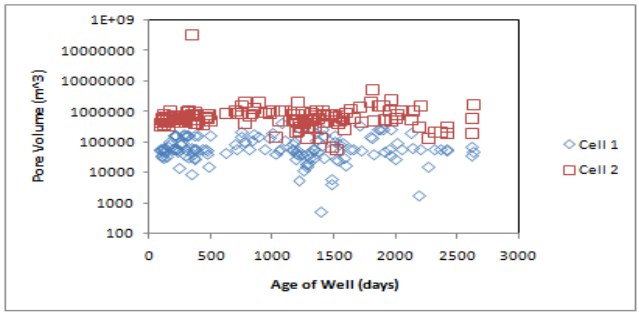

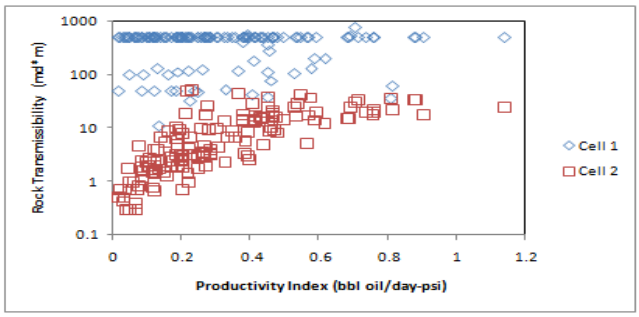

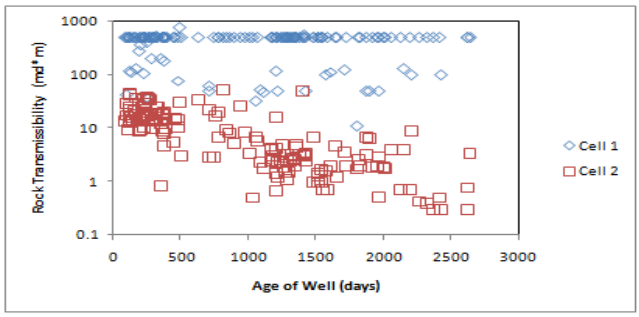

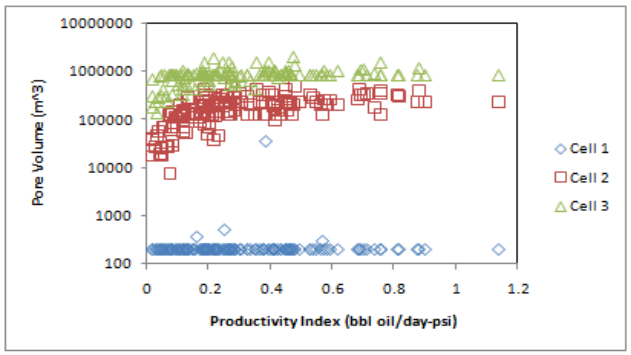
Pore Volume (m^3)
10000000
1000000
100000
10000
1000
100
0
0.2
0.4
0.6
0.8
1
1.2
Productivity Index (bbl oil/day-psi)
Cell 1
Cell 2
Cell 3

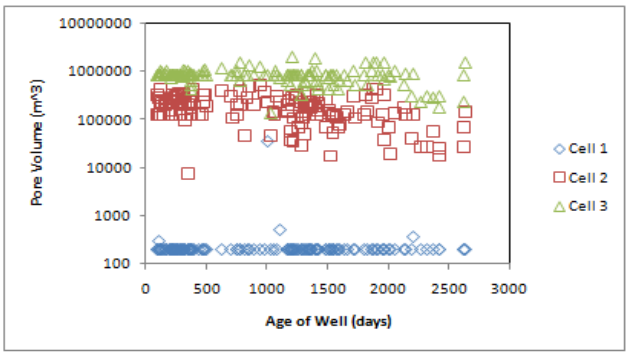
Pore Volume (m^3)
10000000
1000000
100000
10000
1000
100
0
500
1000
1500
2000
2500
3000
Age of Well (days)
Cell 1
Cell 2
Cell 3

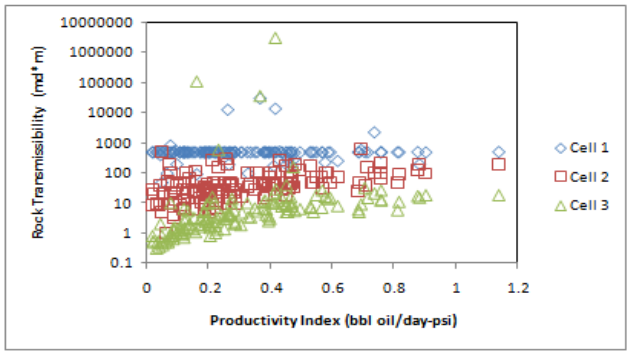
Rock Transmissibility (md* m)
10000000
1000000
100000
10000
1000
100
10
1
0.1
0
0.2
0.4
0.6
0.8
1
1.2
Productivity Index (bbl oil/day-psi)
Cell 1
Cell 2
Cell 3

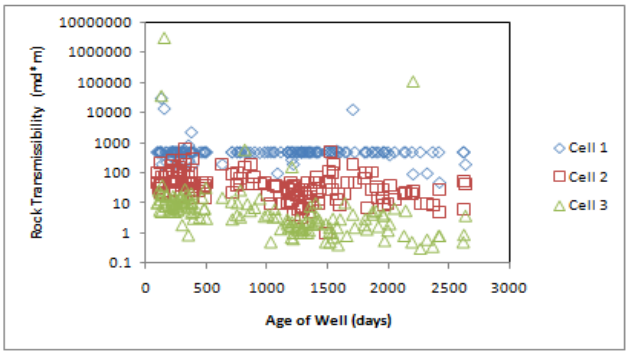
Rock Transmissibility (md* m)
10000000
1000000
100000
10000
1000
100
10
1
0.1
0
500
1000
1500
2000
2500
3000
Age of Well (days)
Cell 1
Cell 2
Cell 3

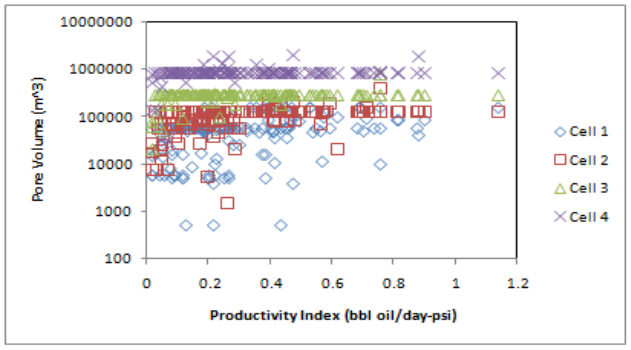
Pore Volume (m^3)
10000000
1000000
100000
10000
1000
100
0
0.2
0.4
0.6
0.8
1
1.2
Productivity Index (bbl oil/day-psi)
Cell 1
Cell 2
Cell 3
Cell 4

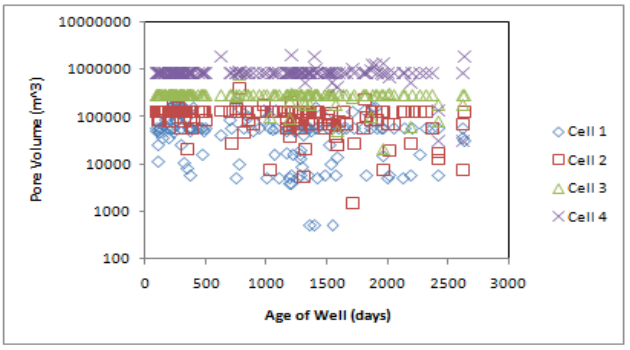
Pore Volume (m^3)
10000000
1000000
100000
10000
1000
100
0
500
1000
1500
2000
2500
3000
Age of Well (days)
Cell 1
Cell 2
Cell 3
Cell 4

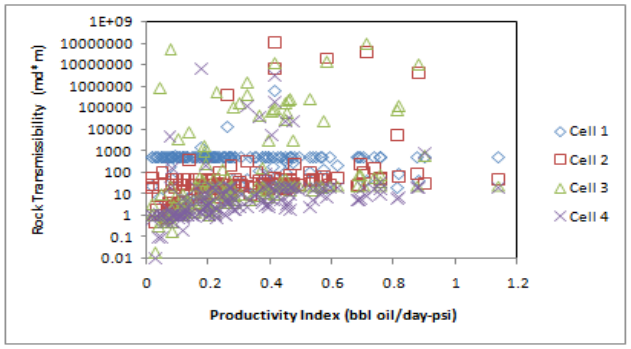
Rock Transmissibility (md* m)
1E+09
10000000
10000000
1000000
100000
10000
1000
100
10
1
0.1
0.01
0
0.2
0.4
0.6
0.8
1
1.2
Productivity Index (bbl oil/day-psi)
Cell 1
Cell 2
Cell 3
Cell 4

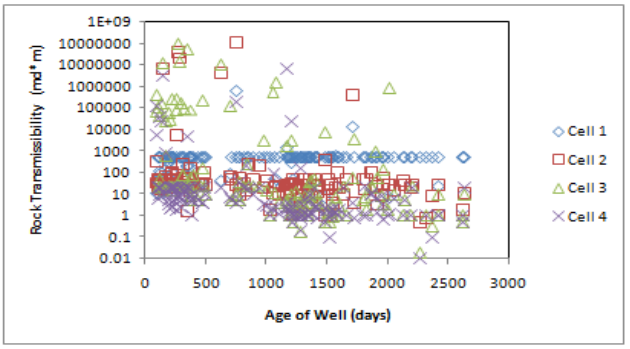
Rock Transmissibility (md* m)
1E+09
10000000
10000000
1000000
100000
10000
1000
100
10
1
0.1
0.01
0
500
1000
1500
2000
2500
3000
Age of Well (days)
Cell 1
Cell 2
Cell 3
Cell 4

APPENDIX C

Modeled pore volume vs. various well summary data

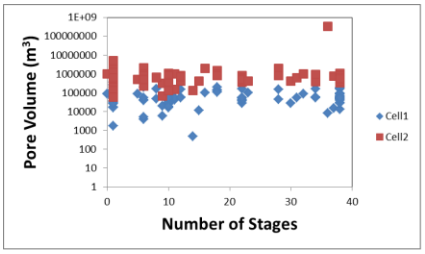

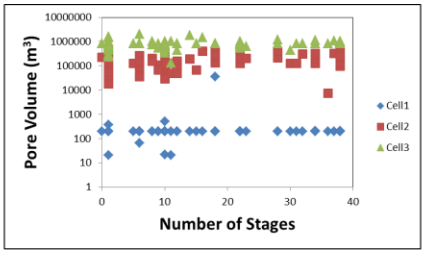

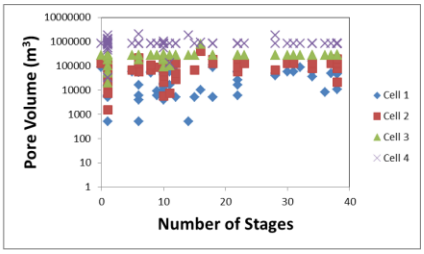

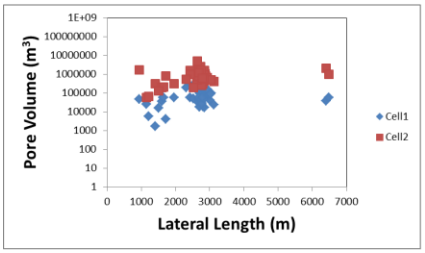

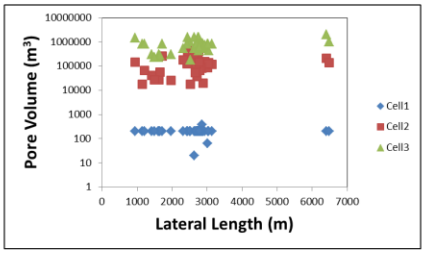

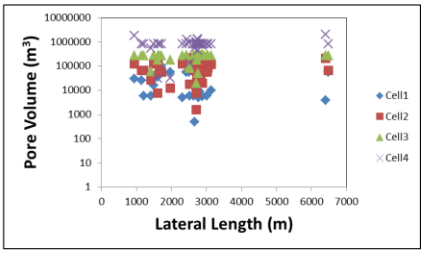

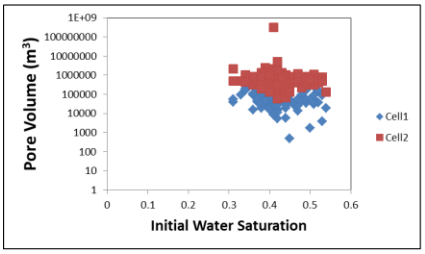

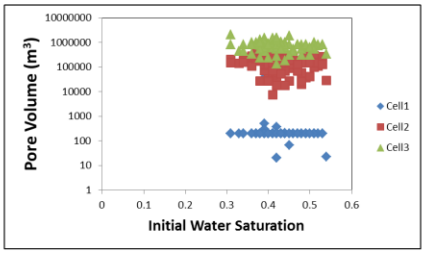

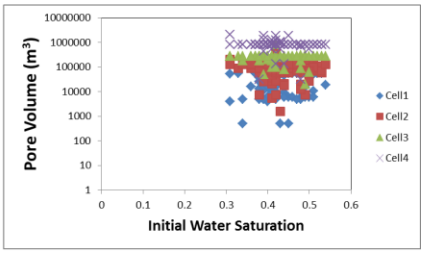

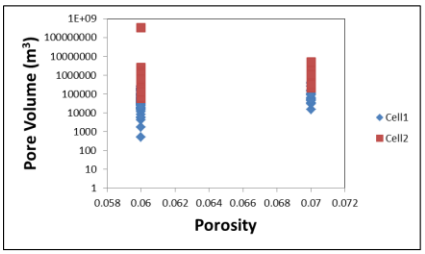

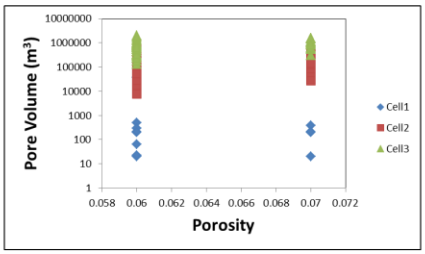

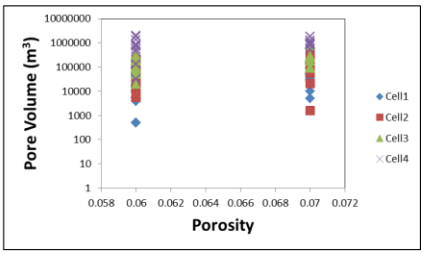

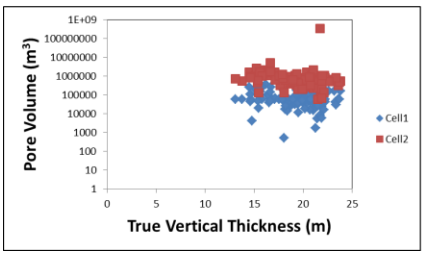

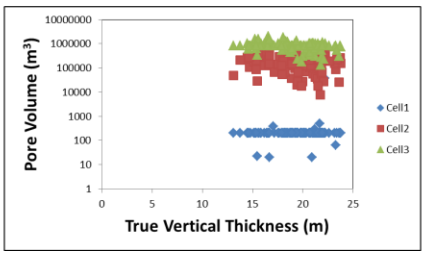

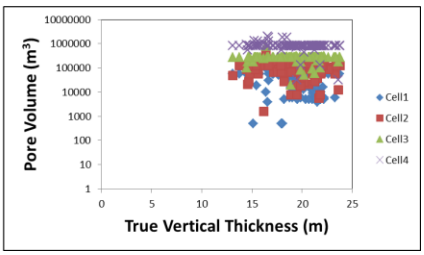

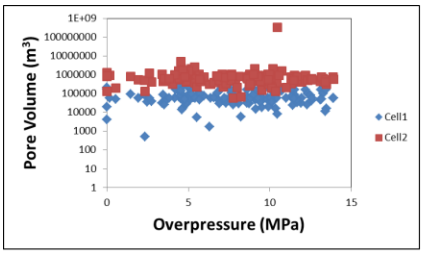
Pore Volume (m³)
Overpressure (MPa)
Cell1
Cell2

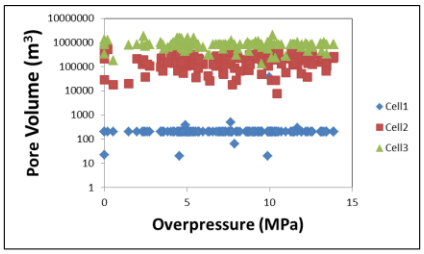
Pore Volume (m³)
Overpressure (MPa)
Cell1
Cell2
Cell3

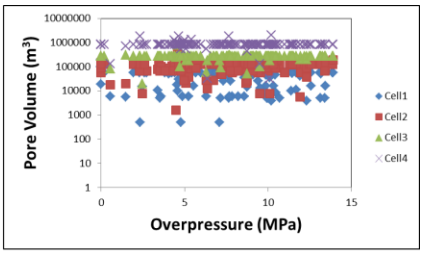
Pore Volume (m³)
Overpressure (MPa)
Cell1
Cell2
Cell3
Cell4

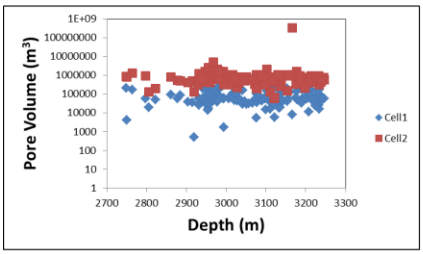
Pore Volume (m³)
Depth (m)
Cell1
Cell2

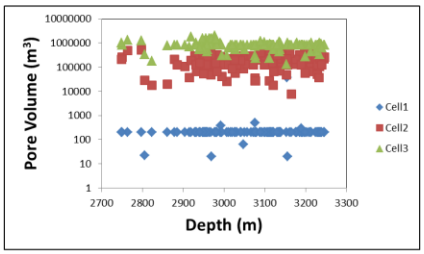
Pore Volume (m³)
Depth (m)
Cell1
Cell2
Cell3

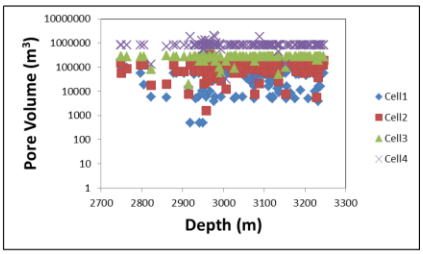
Pore Volume (m³)
Depth (m)
Cell1
Cell2
Cell3
Cell4

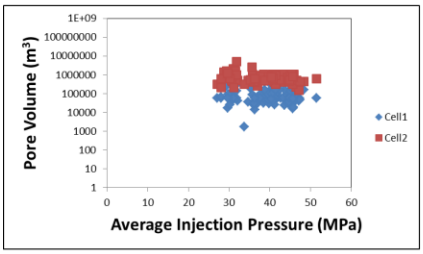
Pore Volume (m³)
Average Injection Pressure (MPa)
Cell1
Cell2

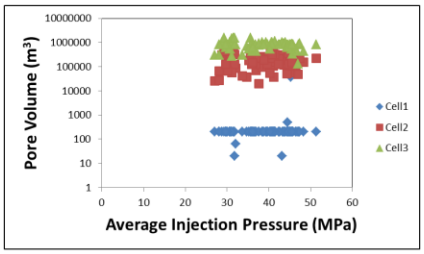
Pore Volume (m³)
Average Injection Pressure (MPa)
Cell1
Cell2
Cell3

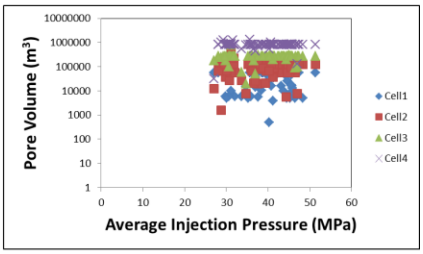
Pore Volume (m³)
Average Injection Pressure (MPa)
Cell1
Cell2
Cell3
Cell4

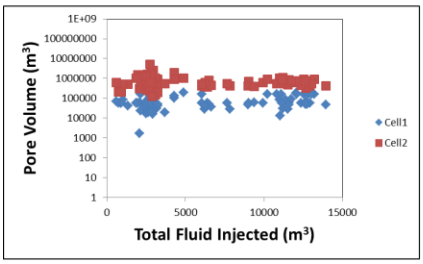
Pore Volume (m³)
Total Fluid Injected (m³)
Cell1
Cell2

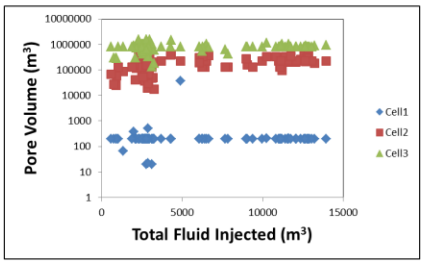
Pore Volume (m³)
Total Fluid Injected (m³)
Cell1
Cell2
Cell3

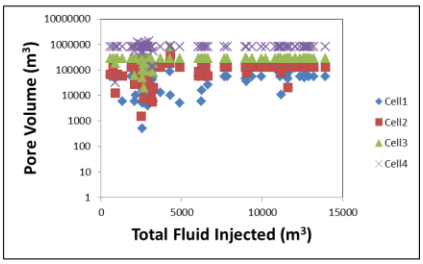
Pore Volume (m³)
Total Fluid Injected (m³)
Cell1
Cell2
Cell3
Cell4

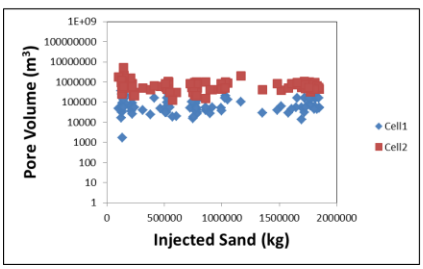
Pore Volume (m³)
Injected Sand (kg)
Cell1
Cell2

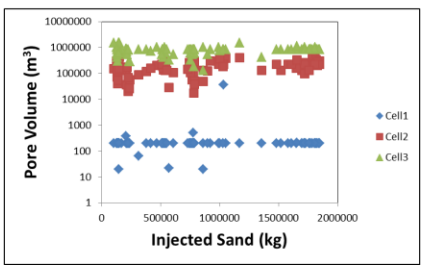
Pore Volume (m³)
Injected Sand (kg)
Cell1
Cell2
Cell3

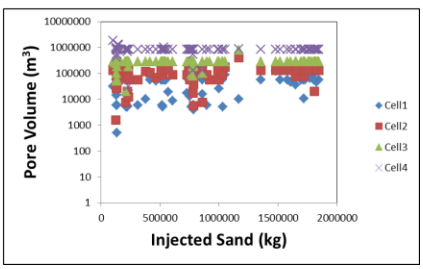
Pore Volume (m³)
Injected Sand (kg)
Cell1
Cell2
Cell3
Cell4

APPENDIX D

Modeled transmissibility vs. various well summary data

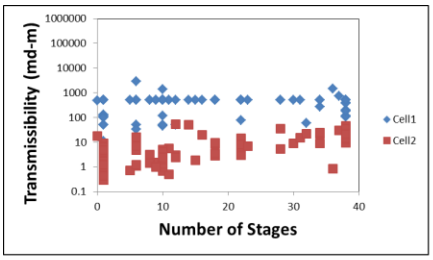

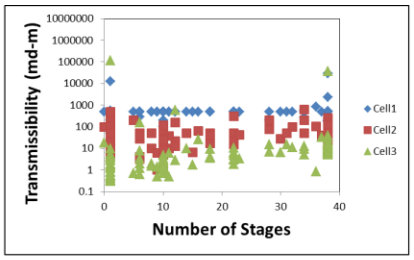

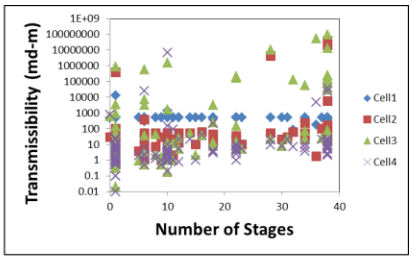

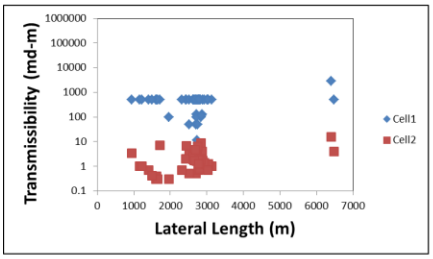

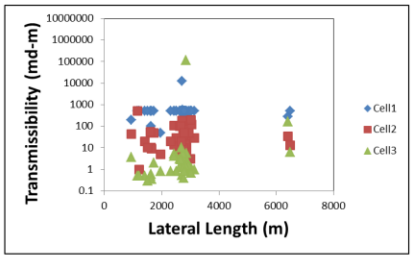

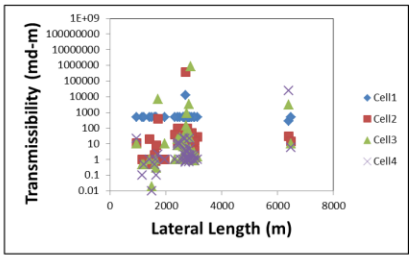

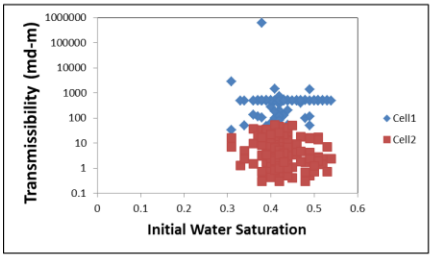

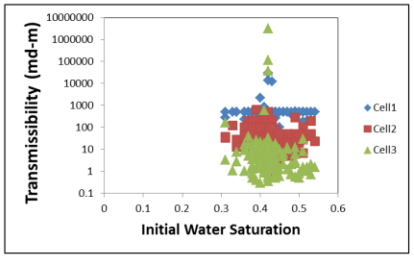

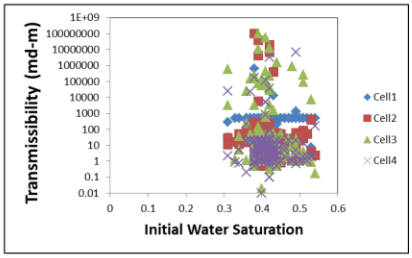

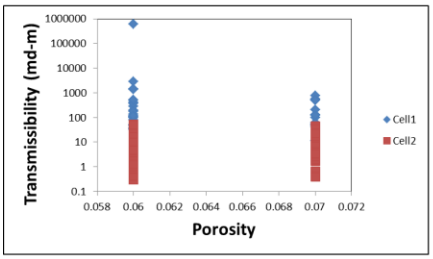

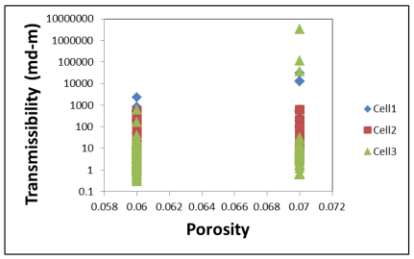

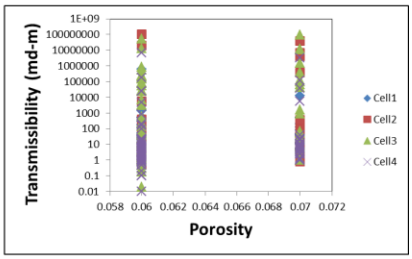

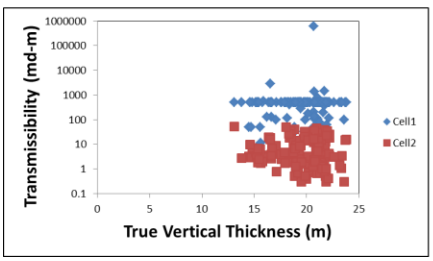

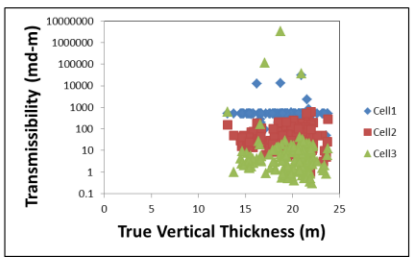

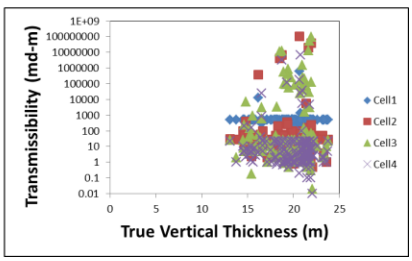

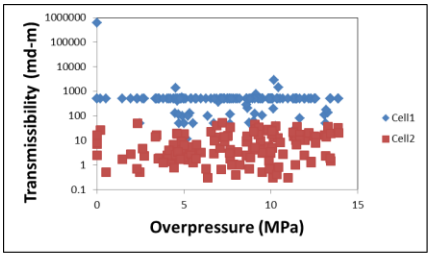
Transmissibility (md-m)
Overpressure (MPa)
Cell1
Cell2

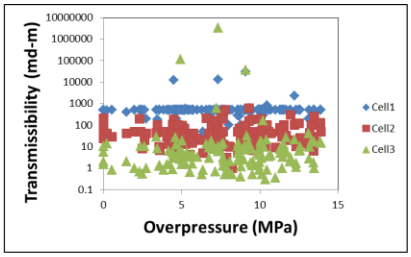
Transmissibility (md-m)
Overpressure (MPa)
Cell1
Cell2
Cell3

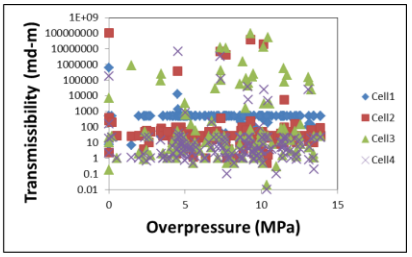
Transmissibility (md-m)
Overpressure (MPa)
Cell1
Cell2
Cell3
Cell4

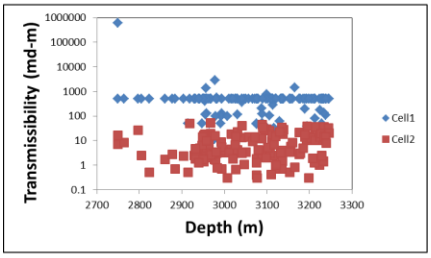
Transmissibility (md-m)
Depth (m)
Cell1
Cell2

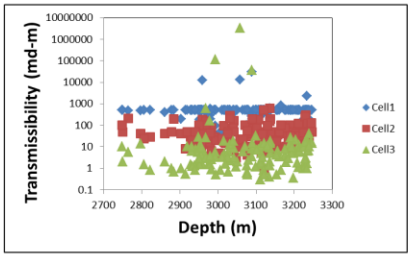
Transmissibility (md-m)
Depth (m)
Cell1
Cell2
Cell3

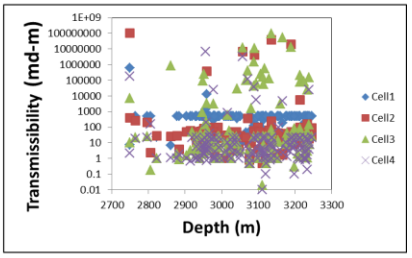
Transmissibility (md-m)
Depth (m)
Cell1
Cell2
Cell3
Cell4

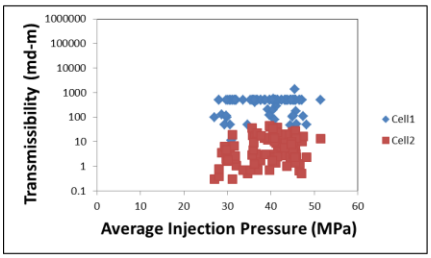
Transmissibility (md-m)
Average Injection Pressure (MPa)
Cell1
Cell2

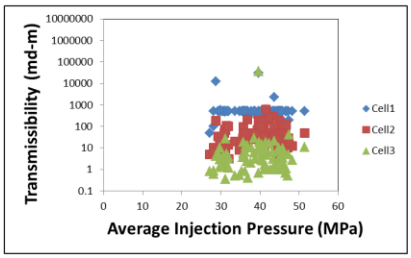
Transmissibility (md-m)
Average Injection Pressure (MPa)
Cell1
Cell2
Cell3

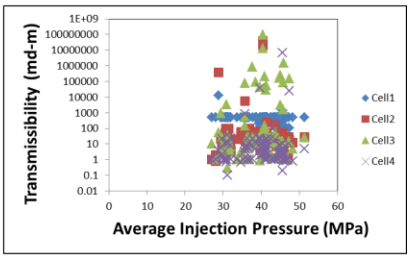
Transmissibility (md-m)
Average Injection Pressure (MPa)
Cell1
Cell2
Cell3
Cell4

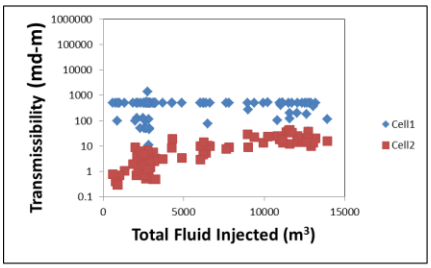
Transmissibility (md-m)
Total Fluid Injected (m³)
Cell1
Cell2

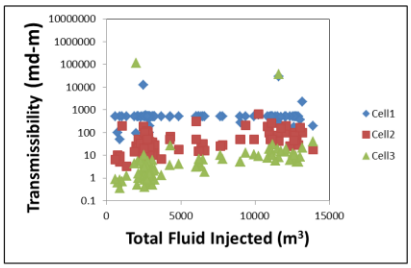
Transmissibility (md-m)
Total Fluid Injected (m³)
Cell1
Cell2
Cell3

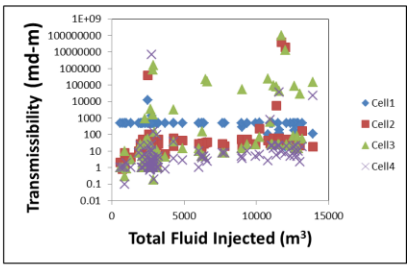
Transmissibility (md-m)
Total Fluid Injected (m³)
Cell1
Cell2
Cell3
Cell4

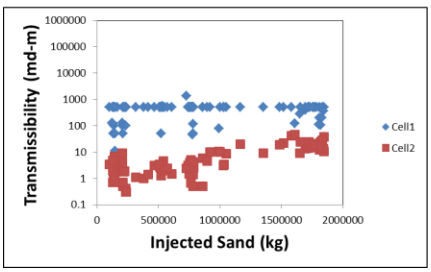
Transmissibility (md-m)
Injected Sand (kg)
Cell1
Cell2

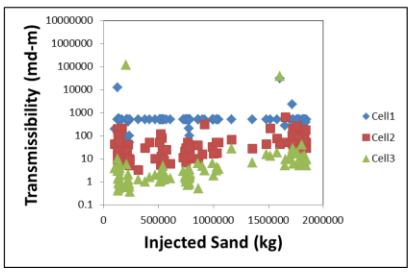
Transmissibility (md-m)
Injected Sand (kg)
Cell1
Cell2
Cell3

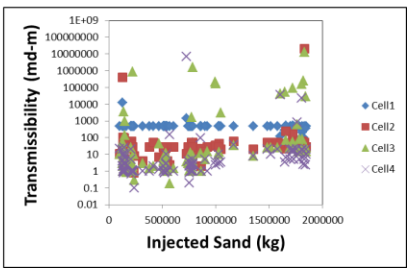
Transmissibility (md-m)
Injected Sand (kg)
Cell1
Cell2
Cell3
Cell4

APPENDIX E

Comparison of using 1 cell vs 2 cells to model the oil production data.

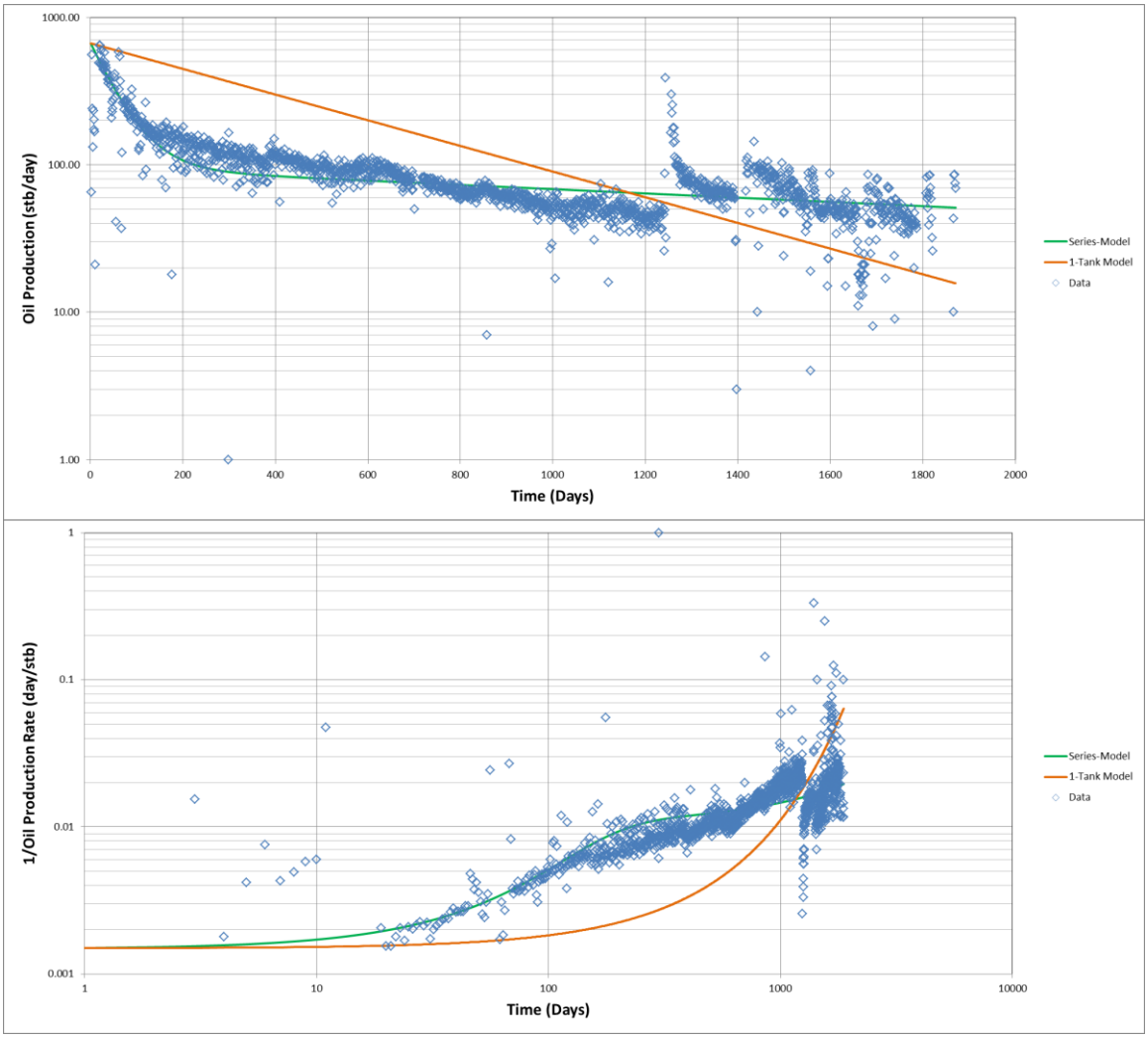

Daily oil production data set from well UTID: 4 was modeled using 1 cell and 2 cells. The models are compared on the oil production (log scale) vs. time and 1/oil production rate (log scale) vs. time (log scale) plots above.

When just 1 cell is used to model the production data a straight line is made on the oil production (log scale) vs. time plot; this is consistent with the idea of a single tank experiencing

exponential production decline. This straight line formed by the single cell model does not fit the data as well as the model created using 2 cells. Also, the 2 cell model fits the flow regimes as shown in the 1/oil production rate (log scale) vs. time (log scale) plot, where the model generated using 1 cell does not.

At least 2 cells are needed to fit the production data from this dataset.

APPENDIX F

Mass Balance Derivation Showing the Relationship Between $\frac{dP}{dx}$ and Time inside a Fracture Modeled as a 1-D Flow

Variables

$\phi = porosity$
$\rho = density_{oil}$
$\mu = vis\cos ity_{oil}$
$\alpha = diffusivity$
$q = flowrate$
$A = area_{cross-section}$
$u = flux$
$t = time$
$c_t = compressiblility_{total}$
$c_o = compressibility_{oil}$
$c_f = compressibility_{formation}$

Start with the mass balance form of slightly compressible oil:

$$\frac{\partial(\phi\rho)}{\partial t} + \frac{\partial(\rho u)}{\partial x} = 0 \qquad \text{(A)}$$

Where the left side of Equation A accounts for the accumulation term and the right side accounts for the in/out term. Using the chain rule Equation A can be manipulated into Equation B:

$$\phi\frac{\partial\rho}{\partial t} + \rho\frac{\partial\phi}{\partial t} + \frac{\partial(\rho u)}{dx} = 0$$

$$\phi\frac{\partial\rho}{\partial P}\frac{\partial P}{\partial t} + \rho\frac{\partial\phi}{\partial P}\frac{\partial P}{\partial t} + \frac{\partial(\rho u)}{dx} = 0$$

$$(\phi\frac{\partial\rho}{\partial P}+\rho\frac{\partial\phi}{\partial P})\frac{\partial P}{\partial t}+\frac{\partial(\rho u)}{dx}=0$$

$$(\phi\rho\frac{1}{\rho}\frac{\partial\rho}{\partial P}+\rho\phi\frac{1}{\phi}\frac{\partial\phi}{\partial P})\frac{\partial P}{\partial t}+\frac{\partial(\rho u)}{dx}=0 \qquad \text{(B)}$$

At this point we recognize that the oil compressibility, formation compressibility, and total compressibility are defined as:

$$c_o=\frac{1}{\rho}\frac{\partial\rho}{\partial P}$$

$$c_f=\frac{1}{\phi}\frac{\partial\phi}{\partial P}$$

$$c_t=c_o+c_f$$

When the compressibility definitions are applied to Equation B:

$$(\phi\rho c_o+\rho\phi c_f)\frac{\partial P}{\partial t}+\frac{\partial(\rho u)}{dx}=0$$

$$c_t\phi\rho\frac{\partial P}{\partial t}+\frac{\partial(\rho u)}{dx}=0 \qquad \text{(C)}$$

According to Darcy's Law, the flux (u) is defined as:

$$u=\frac{q}{A}=\frac{k}{\mu}\frac{\partial P}{\partial x}$$

Substitute Darcy's Law to Equation C:

$$c_t\phi\rho\frac{\partial P}{\partial t}+\frac{\partial}{dx}(\frac{k}{\mu}\frac{\partial P}{\partial x})=0$$

$$c_t\phi\rho\frac{\partial P}{\partial t}+\frac{k}{\mu}(\rho\frac{\partial}{\partial x}(\frac{\partial P}{\partial x})+\frac{\partial P}{\partial x}\frac{\partial\rho}{\partial x})=0$$

$$c_t\phi\rho\frac{\partial P}{\partial t}+\rho\frac{k}{\mu}(\frac{\partial^2 P}{\partial x^2}+\frac{1}{\rho}\frac{\partial\rho}{\partial P}\frac{\partial P}{\partial x}\frac{\partial P}{\partial x})=0$$

Once again applying the definition of oil compressibility:

$$c_t\phi\rho\frac{\partial P}{\partial t}+\rho\frac{k}{\mu}(\frac{\partial^2 P}{\partial x^2}+c_o(\frac{\partial P}{\partial x})^2)=0 \qquad \text{(D)}$$

As this derivation is for a slightly compressible oil, we assume that:

$$c_o(\frac{\partial P}{\partial x})^2=0$$

Equation D becomes:

$$c_t\phi\rho\frac{\partial P}{\partial t}+\rho\frac{k}{\mu}(\frac{\partial^2 P}{\partial x^2})=0$$

$$c_t\phi\frac{\partial P}{\partial t}+\frac{k}{\mu}(\frac{\partial^2 P}{\partial x^2})=0 \qquad \text{(E)}$$

If we define diffusivity as:

$$\alpha=\frac{k}{\phi\mu c_t}$$

We can get the continuity equation for a slightly compressible oil in 1-D (Equation F).

$$\frac{1}{\alpha}\frac{\partial P}{\partial t}+\frac{\partial^2 P}{\partial x^2}=0 \qquad \text{(F)}$$

For the following solution to the continuity equation, we need boundary conditions and a similarity transform.

The assumptions used in this solution are:

1) Constant pressure at the well

$$P(0,t)=P_0$$

2) Pressure in the formation is uniform initially

$$P(x,0) = P_i$$

3) The pressure far(infinitely) away is equal to the initial formation pressure (this assumption assumes infinite drainage length)

$$P(\infty,t) = P_i$$

The similarity transform used in this solution is:

$$\eta = \frac{x}{2\sqrt{\alpha t}} \tag{G}$$

From this similarity variable,

$$\frac{\partial P}{\partial t} = \frac{\partial P}{\partial \eta}\frac{\partial \eta}{\partial t}$$

$$\frac{\partial P}{\partial t} = \frac{\partial P}{\partial \eta}\frac{\partial}{\partial t}\left(\frac{x}{2\sqrt{\alpha t}}\right)$$

$$\frac{\partial P}{\partial t} = \frac{x}{2\sqrt{\alpha}}\frac{\partial P}{\partial \eta}\left(-\frac{1}{2}t^{-3/2}\right)$$

$$\frac{\partial P}{\partial t} = -\frac{x}{4\sqrt{\alpha t}}\frac{1}{t}\frac{\partial P}{\partial \eta}$$

$$\frac{\partial P}{\partial t} = -\frac{\eta}{2t}\frac{\partial P}{\partial \eta} \tag{H}$$

$$\frac{\partial P}{\partial x} = \frac{\partial P}{\partial \eta}\frac{\partial \eta}{\partial x}$$

$$\frac{\partial P}{\partial x} = \frac{\partial P}{\partial \eta}\frac{\partial}{\partial x}\left(\frac{x}{2\sqrt{\alpha t}}\right)$$

$$\frac{\partial P}{\partial x} = \frac{\partial P}{\partial \eta}\frac{1}{2\sqrt{\alpha t}} \tag{I}$$

$$\frac{\partial^2 P}{\partial x^2} = \frac{\partial}{\partial \eta}\frac{\partial \eta}{\partial x}\frac{\partial P}{\partial x}$$

$$\frac{\partial^2 P}{\partial x^2} = \frac{\partial}{\partial \eta}\frac{\partial \eta}{\partial x}\frac{\partial P}{\partial \eta}\frac{1}{2\sqrt{\alpha t}}$$

$$\frac{\partial^2 P}{\partial x^2} = \frac{1}{4\alpha t}\frac{\partial^2 P}{\partial \eta^2}$$

Also the boundary conditions would transform to:

$$P(\eta = 0) = P_0 \tag{J}$$

$$P(\eta = \infty) = P_i \tag{K}$$

When the similarity transform is applied to the continuity equation (Equation F):

$$\frac{1}{\alpha}\left(-\frac{\eta}{2t}\frac{\partial P}{\partial \eta}\right) + \frac{1}{4\alpha t}\frac{\partial^2 P}{\partial \eta^2} = 0 \tag{L}$$

Equation L can be rearranged into a 2nd order ordinary differential equation:

$$\frac{\partial^2 P}{\partial \eta^2} = -2\eta\frac{\partial P}{\partial \eta} \tag{M}$$

When we solve for *P* in Equation M:

$$P(\eta) = \sqrt{\pi}C_1 erf(\eta) + C_2 \tag{O}$$

Applying the transformed boundary conditions (Equation J and K):

$$C_1 = \frac{P_i - P_0}{\sqrt{\pi}}$$

$$C_2 = P_0$$

Thus Equation O becomes:

$$P(\eta) = (P_i - P_0)erf(\eta) + P_0 \qquad \text{(P)}$$

Equation P can be rewritten as:

$$P(\eta) = P_i + (P_i - P_0)erfc(\eta)$$

$$P(x,t) = P_i + (P_i - P_0)erfc(\frac{x}{2\sqrt{\alpha t}}) \qquad \text{(Q)}$$

When we solve for $\frac{dP}{dx}$:

$$\frac{dP}{dx} = (P_i - P_0)(-\frac{e^{\frac{-x^2}{4\alpha t}}}{\sqrt{\pi\alpha t}}) \qquad \text{(R)}$$

At the wellbore, $x \to 0$. So Equation R becomes:

$$\frac{dP}{dx} = (P_i - P_0)(-\frac{1}{\sqrt{\pi\alpha t}}) \qquad \text{(S)}$$

This derivation demonstrates the relationship between the pressure drop and time near the wellbore.

REFERENCES

Agboada, D., &Ahmadi, M. "Production Decline and Numerical Simulation Model Analysis of the Eagle Ford Shale Oil Play." SPE 165315 presented at the SPE Western Regional & AAPG Pacific Section Meeting, 2013 Joint Technical Conference held in Monterey, California, USA (Sep 19-25, 2013).

Arps, J. "Analysis of Decline Curves." Transactions of the AIME, Houston Meeting (May 1945).

Besler, M., Steele, J., Egan, T., & Wagner, J. "Improving Well Productivity and Profitability in the Bakken - A Summary of Our Experiences Drilling, Stimulating, and Operating Horizontal Wells." SPE 110679 presented at the 2007 SPE Annual Technical Conference and Exhibition held in Anaheim, California, USA (Nov 11-14, 2007).

Cinco-Ley, H. "Evaluation of Hydraulic Fracturing By Transient Pressure Analysis Methods."SPE 10043 presented at the International Petroleum Exhibition and Technical Symposium of the Society of Petroleum Engineers held in Beijing, China (Mar 18-26, 1982).

Cinco-Ley, H., Ramey Jr., H., Samaniego, F., & Rodriguez, F. "Behavior of Wells With Low-Conductivity Vertical Fractures." SPE 16776 presented at the 62nd Annual Technical Conference and Exhibition of the Society of Petroleum Engineers held in Dallas, TX, USA (Sep 27-30, 1987).

Clark, A., Lake, L., &Patzek, T. "Production Forecasting with Logistic Growth Models." SPE 144790 presented at the SPE Annual Technical Conference and Exhibition held in Denver, Colorado, USA (Oct 30-Nov 2, 2011).

Eisinger, C., & Milne, J. Niobrara Tight Oil Success in Colorado: What Do The Numbers Indicate? Grand Junction, Colorado: AAPG Rocky Mountain Selection Meeting, (2012).

Energy Information Administration. Lower 48 States Shale Plays. (2011). <http://www.eia.gov/oil_gas/rpd/shale_gas.jpg>.

Foran, S. Fracking-Good News or Bad for America's Energy Needs? (2011). <http://today.uconn.edu/blog/2011/12/fracking-%E2%80%93-good-news-or-bad-for-america%E2%80%99s-energy-needs/>.

Kabir, C., Rasdi, F., &Igboalisi, B. "Analyzing Production Data From Tight Oil Wells." Journal of Canadian Petroleum Technology, Volume 50, Number 5 (May 2011): 48-58.

Kanfar, M., &Wattenbarger, R. "Comparison of Empirical Decline Curve Methods for Shale Wells." SPE 162648 presented at the SPE Canadian Unconventional Resources Conference held in Calgary, Alberta, Canada (Oct 30-Nov 1, 2012).

Kumar, S., Hoffman, T., & Prasad, M. "Upper and Lower Bakken Shale Production Contribute to the Middle Bakken Reservoir." SPE 168797/URTeC 151459 presented at the Unconventional Resources Technology Conference held in Denver, Colorado, USA (Aug, 12-14, 2013).

Lake, L. W. “Excerpt from Reservoir Engineering Class Notes." (2013).

Lyle, D. Shale Gas Plays Explained. (2007). <http://www.epmag.com/archives/features/304.htm>.

Maugeri, L. "The Shale Oil Boom: A U.S. Phenomenon." Harvard Kennedy School Belfer Center for Science and International Affairs (2013).

Miller, M., Jenkins, C., &Rai, R. "Applying Innovative Production Modeling Techniques to Quantify Fracture Characteristics, Reservoir Properties, and Well Performance in Shale Gas Reservoirs." SPE 139097 presented at the SPE Eastern Regional Meeting held in Morgantown, West Virginia, USA (Oct 12-14, 2010).

Mills, K., Jeffery, R., &Xhang, X. "Growth Analysis and Fracture Mechanics Based on Measured Stress Change Near a Full-Size Hydraulic Fracture." ARMA/NARMS 04-521 presented at Gulf Rocks 2004, the 6th North America Rock Mechanics Symposium, held in Houston, Texas (June 5-9, 2004).

North Dakota Department of Mineral Resources. ND Monthly Bakken Oil Production Statistics. (2013). <https://www.dmr.nd.gov/oilgas/stats/historicalbakkenoilstats.pdf>.

Paige, R., Roberts, J., Murray, L., & Mellor, D. "Fracture Measurement Using Hydraulic Impedance Testing." SPE 24824 presented at the 67th Annual Technical Conference and Exhibition of the Society of Petroleum Engineers held in Washington, DC (Oct 4-7, 1992).

Sonnenberg, S. "New Reserves in an Oil Field, the Niobrara Resource Play in the Wattenberg Field, Denver Basin, Colorado." SPE 145684 presented at the Unconventional Resources Technology Conference held in Denver, Colorado, USA (Aug 12-14, 2013).

Spencer, J., Bucior, D., Catlett, R., &Lolon, E. "Evaluation of Horizontal Wells in the Eagle Ford Using Oil-Based Chemical Tracer Technology to Optimize Stimulation Design." SPE 163846 presented at the 2013 SPE Hydraulic Fracturing Technology Conference held in The Woodlands, Texas, USA, (Feb, 4-6, 2013).

Texas Railroad Commission. Texas Eagle Ford Shale Drilling Permits Issued 2008 through October 2013. (2013). <http://www.rrc.state.tx.us/eagleford/EagleFordDrillingPermitsIssued.pdf>.

Tian, Y., & Ayers, W. "Barnett Shale (Mississippian), Fort Worth Basin, Texas: Regional Variations in Gas and Oil Production and Reservoir Properties." CSUG/SPE 137766 presented at the Canadian Unconventional Resources & International Petroleum Conference held in Calgary, Alberta, Canada (Oct 19-21, 2010).

Tian, Y., Ayers, W., & McCain, W. "The Eagle Ford Shale Play, South Texas: Regional Variations in Fluid Types, Hydrocarbon Production and Reservoir Properties." IPTC 16808 presented at the International Petroleum Technology Conference held in Beijing, China (Mar 26-28, 2013).

Timur, G. "Modeling of Hydraulically Fractured Wells in Full Field Reservoir Simulation Model." SPE 117421 presented at the 2008 SPE Russian Oil & Gas Technical Conference and Exhibition held in Moscow, Russia, (Oct 28-30, 2008).

Tran, T., Sinurat, P., &Wattenbarger, B. "Production Characteristics of the Bakken Shale Oil." SPE 145684 presented at the SPE Annual Technical Conference and Exhibition held in Denver, Colorado, USA (Oct 30-November 2, 2011).

U.S. Energy Information Administration.Crude Oil Production.(2013). <http://www.eia.gov/dnav/pet/pet_crd_crpdn_adc_mbblpd_a.htm>.

Valko, P. "Assigning Value to Stimulation in the Barnett Shale: A Simultaneous Analysis of 7000 Plus Production Histories and Well Completion Records." SPE 119369 presented at the 2009 SPE Hydraulic Fracturing Technology Conference held in the Woodlands, Texas, USA (Jan 19-21, 2009).

Yu, S., Lee, J., Miocevic, D., Li, D., & Harris, S. "Estimating Proved Reserves in Tight/Shale Wells Using the Modified SEPD Method." SPE 166198 presented at the SPE Annual Technical Conference and Exhibition held in New Orleans, Louisiana, USA, (Sep 30-Oct 2, 2013).

Yuan, H., Soar, L., Packer, R., Bhuiyan, M., &Jiafu, X. "A Case Study to Evaluate Shale Oil Production Performance Models with Actual Well Production Data." SPE 168842/URTeC 1582234 presented at the Unconventional Resources Technology Conference held in Denver, Colorado, USA (Aug 12-14, 2013).

Zhang, X., Deimbacher, F., Crick, M., &Harikesavanallur, A. "Sensitivity Studies of Horizontal Wells with Hydraulic Fractures in Shale Gas Reservoirs." IPTC 13338 presented at the International Petroleum Technology Conference held in Doha, Qatar (Dec 7-9, 2009).

Zhou, J., Jung, C., Chenevert, M., & Sharma, M. "A Systematic Approach to Petrophysical Characterization of Organic-Rich Shales in Barnett and Eagle Ford Formations." SPE 168792/URTeC 1581323 presented at the Unconventional Resources Technology Conference held in Denver, Colorado, USA (Aug, 12-14, 2013).